Single-blind determination of methane detection limits and quantification accuracy using aircraft-based LiDAR, Supporting Information

Clay Bell[1], Jeff Rutherford[2], Adam Brandt[2], Evan Sherwin[2], Timothy Vaughn[1], Daniel Zimmerle[1]

[1]Energy Institute, Colorado State University, Fort Collins, CO, USA
[2]Department of Energy Resources Engineering, Stanford University, Stanford, CA, USA
[*]clay.bell@colostate.edu

Contents

Interference Testing

Gas Mapping LiDAR (GML) is a spatially resolved, atmospheric trace gas measurement intended to locate and quantify methane emissions. The interfering effects of other gases commonly found in oil and gas service were evaluated in controlled laboratory experiment using the GML system in a bench-top setting, as shown in Figures 1, 2 and 3. A sealed sample-gas cell was placed in the beam path of a stationary GML transceiver (Figure 2) which was trained on target located 125 m away (Figure 3). Alignment of the gas cell was confirmed before and after each test point using both laser detector cards and an IR sensitive video camera; minor adjustments were made as needed.

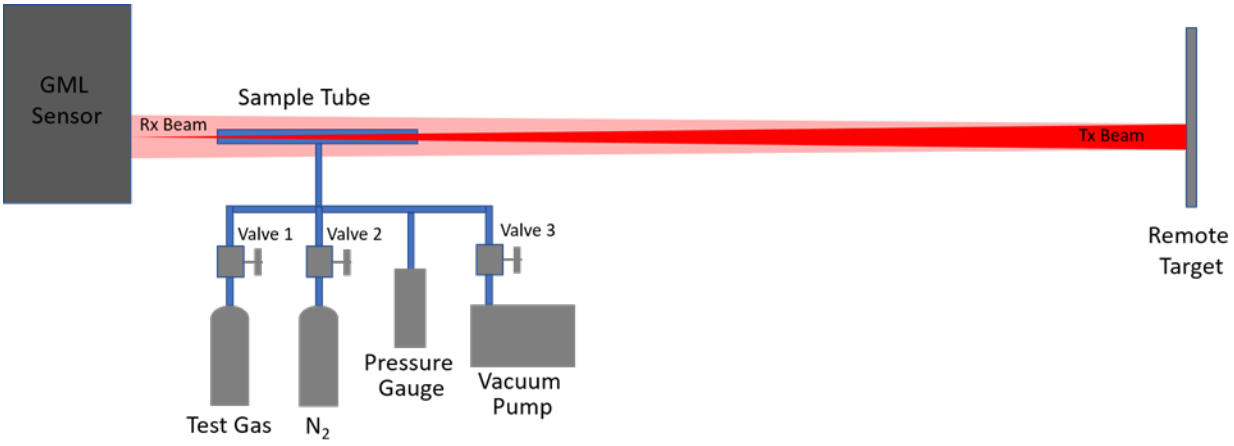

Figure 1. Interference testing experimental schematic. Test gases are introduced to the Sample Tube inserted in-line with the GML Sensor beam.

Before and after each test, the gas cell was vacuum evacuated and filled with industrial grade nitrogen to atmospheric pressure. Measurements were taken to establish a background reading in the absence of test gases and account for atmospheric variation in the remainder of the beam path. For each test, the gas cell was vacuum evacuated and filled to atmospheric pressure with various sample gases blended to the desired volume fraction using partial pressures (Omega Engineering, PX409-015AUSBH). A variety of sample gases were tested. Methane (Oxarc, Industrial Grade, >93 %) was tested at 0.5, 1, 2, and 5 % by volume in nitrogen. Ethylene (Matheson, 99.995 %) was tested at 2, 5, 10, and 20 % by volume in nitrogen. Ethane (Matheson 99.99 %), propane, n-butane, i-butane, (Airgas 99.99 %), and CO_2 (Air Liquide, beverage grade) were each tested at 20 and 50 % by volume in nitrogen, and as pure gases at 100 % by volume. In addition to GML measurements, independent laser absorbance was measured by monitoring laser power (Coherent, FieldMax) at the entrance and exit of the gas cell before each test, as shown in the right most column of Table 1. This provides confirmation that the gas blends are as expected, and illustrates the fundamental methane specificity of the GML laser in the absence of any signal processing or calibration that may occur within the system.

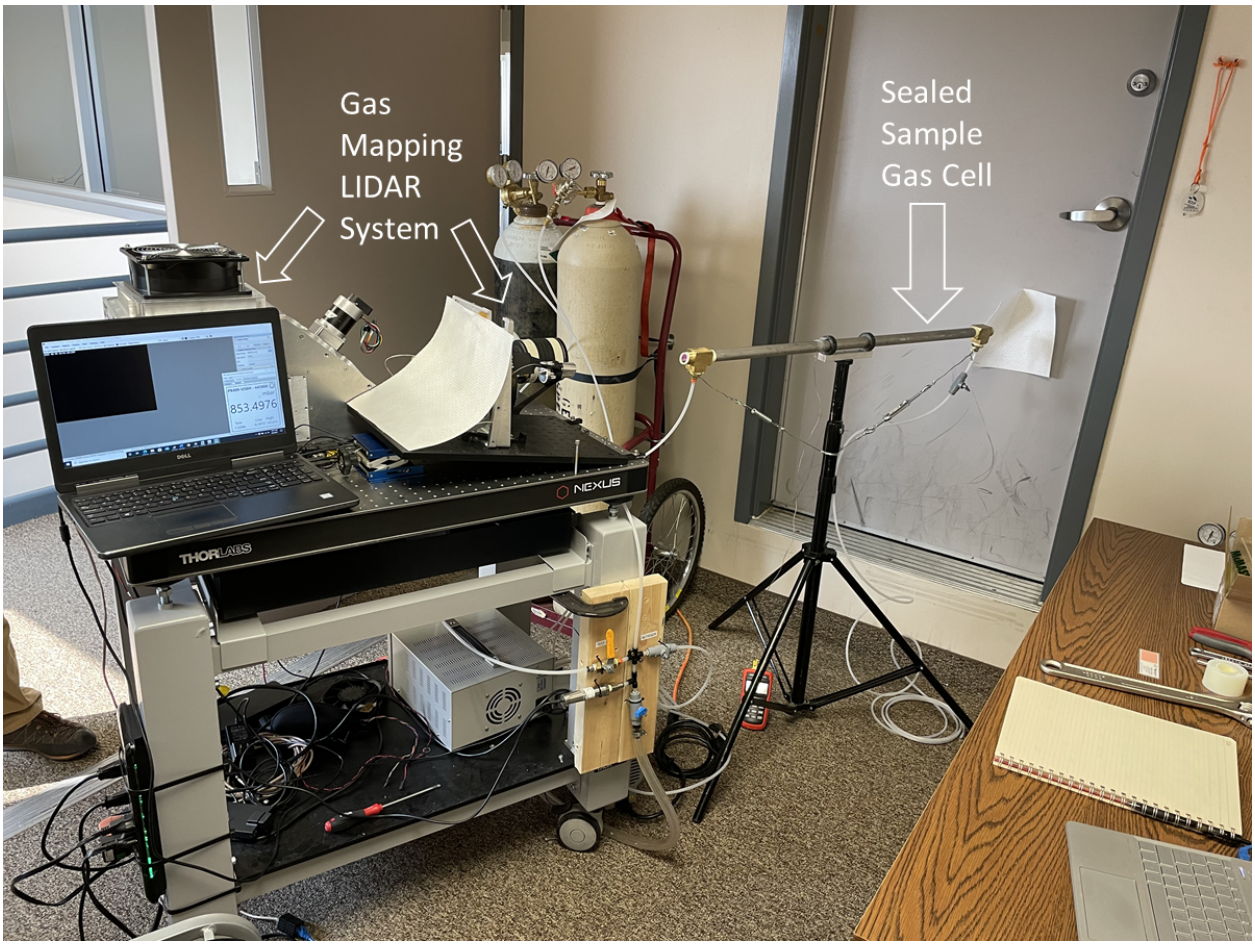

Figure 2. Interference tests were performed using a variety of gas mixtures in a sealed sample-gas cell placed within the beam path of a stationary GML system.

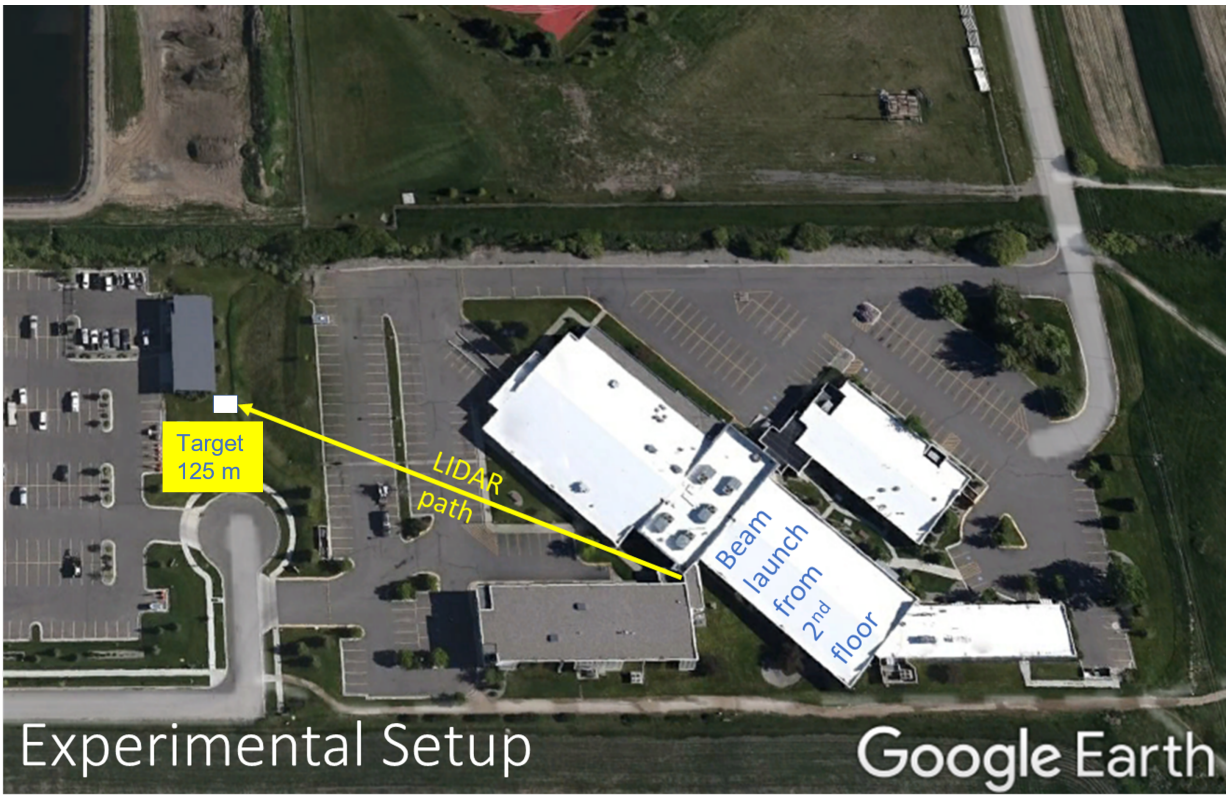

Figure 3. After leaving the gas cell (Figure 2), the GML beam continued to a target (white painted sign) which aided in alignment and reflected the beam back to the GML transceiver uniformly across all tests. A target is not needed in actual field use of the GML sytem.

Results

Measured

Results for GML interference testing are shown in Figure 4. The left panel shows the GML measurement vs the sample gas under test. The right panel shows the associated, independent absorbance measurements. For CO_2, physical absorbance was negligible, as were reported GML results. All hydrocarbon species absorbed some fraction of the transmitted beam, though most had negligible impact on the resulting GML measurement. Only methane, ethylene, and butane showed positive correlations Pearsons R ("R", Table 2). Ordinary least square regressions of GML measurements of these species vs the sample-gas volume fractions tested showed that methane measurements were near-perfect (slope=0.97, R^2=1.0), and that ethylene (slope=0.00179, R^2=0.97) and n-butane (slope=0.000049, R^2=0.89) elicited a small response from the GML system. The very low slope of the regressions indicate weak interference from these species. On average, the ethylene response 500 times weaker than the methane response. On average, the butane response was 20,000 times weaker than the methane response.

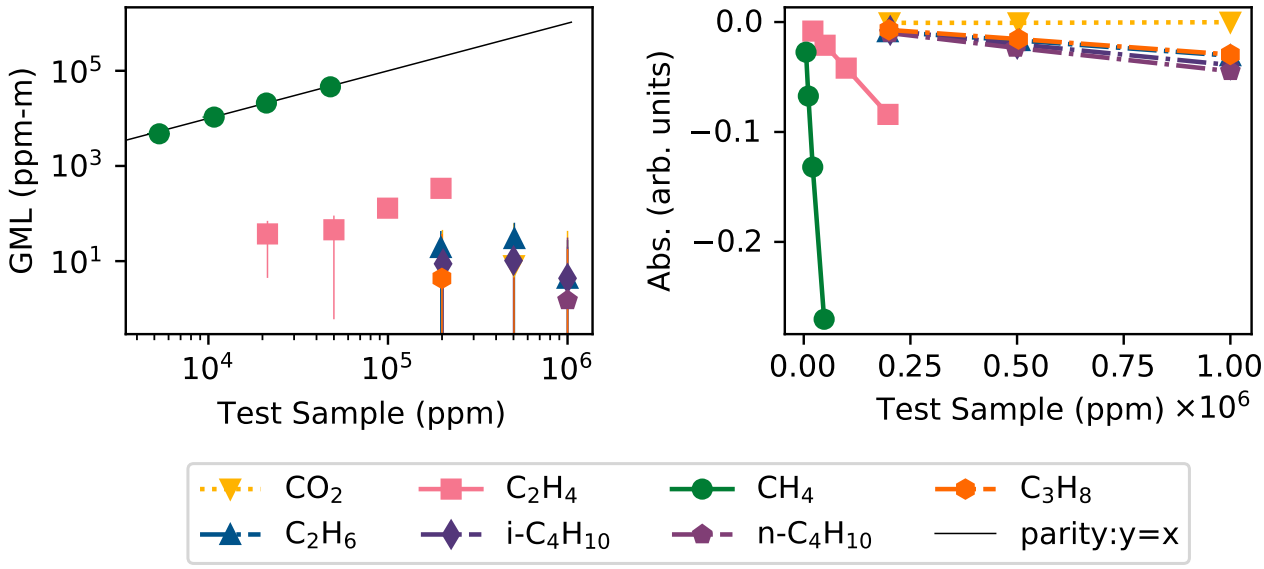

Figure 4. GML interference testing results (left panel) show that methane is strongly correlated, and correctly aligned with the sample-gas volume fraction. Methane is also the strongest absorber of the GML laser (right panel). Ethylene was the strongest absorber of the test gases after methane and elicited a small response from the GML system. Data underlying the figure are shown in Table 1.

Table 1. Interference testing results.

		Test Gas (ppm)		GML Measurement (ppm-m)		Absorbance (arb. units)
Test Gas	Vol %	mean	std	mean	std	mean
Methane	0.5	5324	774	4739	1023	−0.0274
	1.0	10 762	1487	10 635	1771	−0.0673
	2.0	21 041	531	21 000	1488	−0.1319
	5.0	47 805	1472	46 038	3272	−0.2704
Ethylene	2.0	21 332	1536	37	33	−0.0082
	5.0	49 990	928	46	45	−0.0211
	10.0	99 499	252	130	49	−0.0419
	20.0	197 377	5335	339	47	−0.0840
Ethane	20.0	196 934	1891	19	24	−0.0088
	50.0	505 836	8362	30	34	−0.0168
	100.0	1 000 000	0	4	23	−0.0306
Propane	20.0	199 653	3502	4	33	−0.0072
	50.0	503 477	3473	−6	29	−0.0155
	100.0	1 000 000	0	−15	33	−0.0295
n-Butane	20.0	200 898	11 562	−35	22	−0.0100
	50.0	496 156	1793	−34	30	−0.0235
	100.0	1 000 000	0	2	30	−0.0447
i-Butane	20.0	202 713	6007	9	16	−0.0077
	50.0	500 385	3200	10	21	−0.0202
	100.0	1 000 000	0	4	16	−0.0391
CO_2	20.0	201 015	3856	−3	48	−0.0007
	50.0	503 303	7840	8	54	−0.0007
	100.0	1 000 000	0	−4	47	−0.0001

Table 2. Interference testing results fits

Test Gas	Slope	Intercept	R^2	R	R-strength
CO_2	$-4.00 \cdot 10^{-6}$	2.71	0.06	−0.24	negligible correlation
Ethane	$-2.20 \cdot 10^{-5}$	30.15	0.47	−0.70	moderate correlation
Ethylene	$1.79 \cdot 10^{-3}$	−26.96	0.97	0.99	very high correlation
i-Butane	$-6.00 \cdot 10^{-6}$	11.32	0.66	−0.81	high correlation
Methane	$9.66 \cdot 10^{-1}$	90.92	1.0	1.0	very high correlation
n-Butane	$4.90 \cdot 10^{-5}$	−49.87	0.89	0.95	very high correlation
Propane	$-2.40 \cdot 10^{-5}$	8.01	0.98	−0.99	very high correlation

Modeled

To gain insight into the potential for interference from water vapor, SpectraPlot simulations were performed to understand the relative absorption of H_2O and CH_4 at different levels. Two hypothetical examples intended to mimic typical ambient, or gas turbine exhaust conditions were evaluated. For both cases a very weak H_2O absorption feature is present in the wings of the methane feature, as shown in Figure 5.

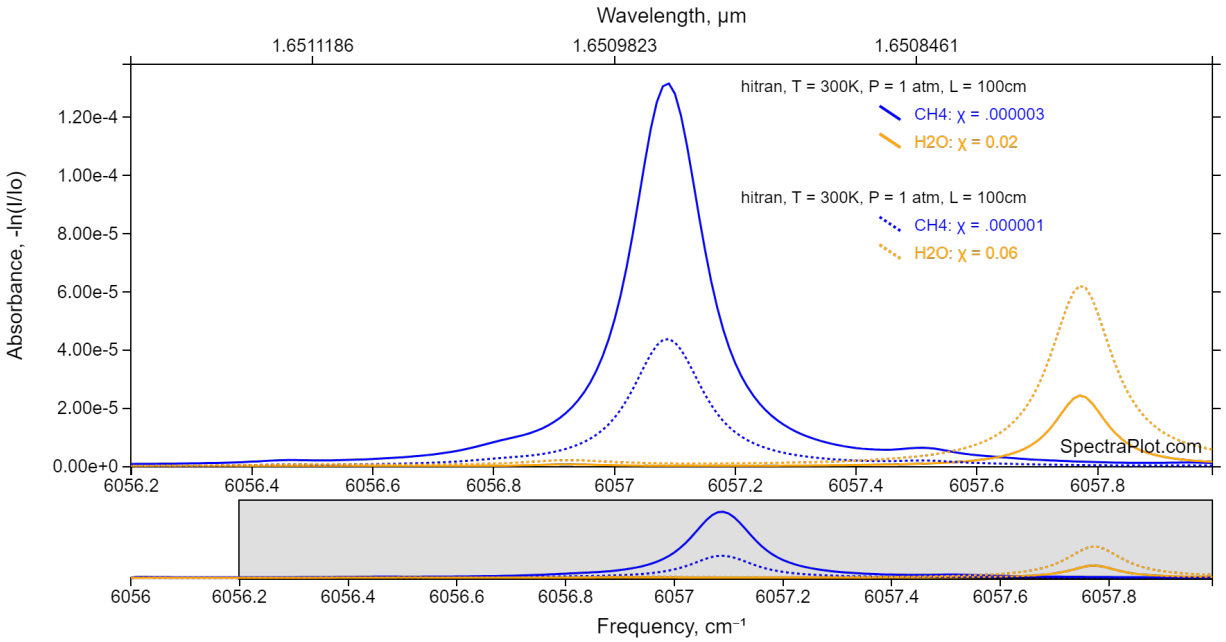

Figure 5. Laboratory interference tests were not performed on H_2O, due to the difficulty of generating moisture samples, but were modeled using SpectraPlot for an "ambient" and "turbine exhaust" case. In both cases the H_2O absorption features were much weaker than the CH_4 absorption features.

Controlled Release Systems

Midland, TX

A schematic and photos of the release system utilized in Midland, Texas are shown in Figure 6 and 7 respectively. A U50 CNG trailer including 16 cylinders with total capacity of 46000 standard cubic feet provided gas to the system. The first stage regulator reduced the pressure from a maximum of 3600 psig to an outlet of approximately 100 psig. The first stage regulator was heated by a catalytic heater to prevent icing. During low flowrate experiments (¡1000 standard cubic feet per hour (scfh)) the catalytic heater was left open to prevent the regulator from overheating. The regulated gas supply was passed through a finned heat exchanger to warm the gas back to ambient temperature after expansion. The U50 trailer was connected to a flow control and metering skid which included two Alicat mass flow controllers (model MCR-250SLPM-D and MCRH-5000SLPM-D-PAR) connected to a lap top for data acquisition and control. Flow data were logged at 1 Hz. Quarter turn valves upstream and downstream of each mass flow controller allowed the flow to be isolated during testing to a single controller. The outlet of the flow control skid was routed to the release point approximately 35 m away (stack coordinates 31.860177°, -102.074091°). The release point was oriented vertically at height of 3.25m Above Ground Level (AGL).

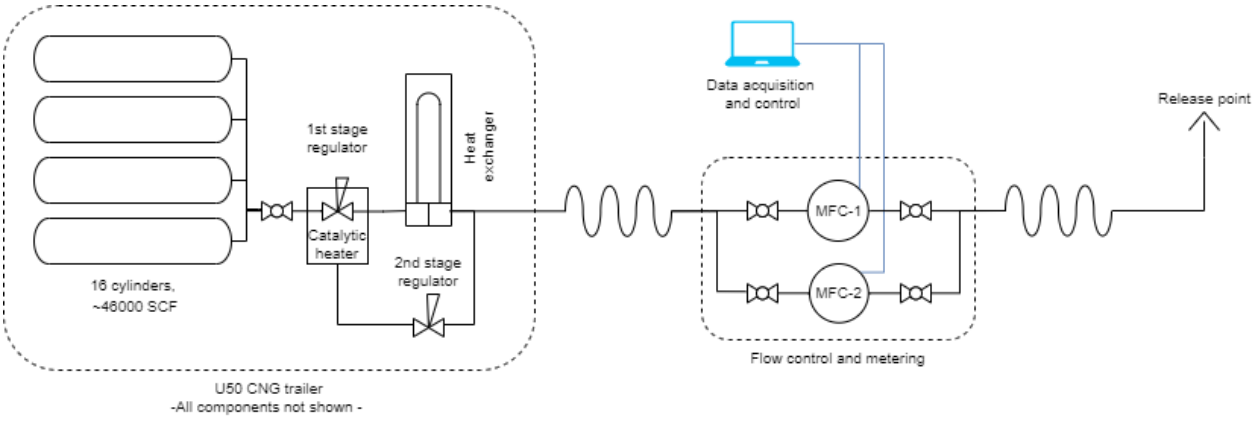

Figure 6. Schematic of release system in Midland, TX.

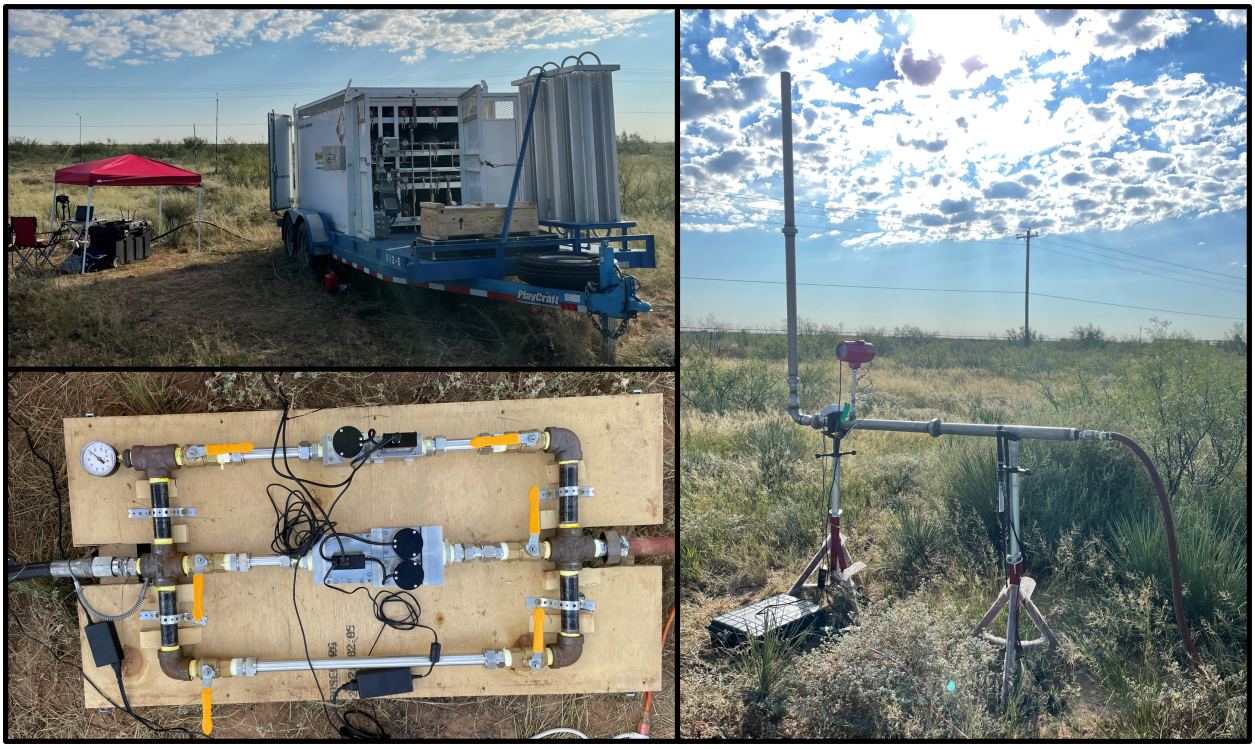

Figure 7. Photos of release system in Midland, TX: U50 CNG trailer and control station (upper left), flow control and metering skid (lower left), and release point (right).)

Ehrenberg, AZ

A detailed description of the Stanford controlled release experiment in Ehrenberg, AZ can be found at Rutherford et al. (2022). A brief summary of the experiment is provided below.

Schematic and photos of the release system in Ehrenberg, AZ are given in Figures 8 and 9, respectively. Gas was supplied by an LNG trailer with rated capacity of 892.3 mscf and working capacity of 800 mscf. The trailer was generally filled to 150 psig. A separate heater trailer, equipped with boilers and a glycol heat exchanger was used to vaporize the LNG to 20- 25 ºC. Flow control was achieved by adjusting a manually loaded regulator to achieve a nominal flow target. After reheating and pressure regulation, gas is transported to the release trailer through an 8 inch hose. The metering and release trailer consists of four parallel pipes of size 0.5 inch, 2 inch, 4 inch, and 8 inch schedule 40 carbon steel pipe. On the 0.5 inch pipe, metering was performed with a Micro Motion ELITE Coriolis meter (ID 21175085). On the remaining three, larger pipes, metering was performed with a Sierra Instruments Quadratherm 640i meter (ID 308188). For redundancy, data was recorded via three separate streams (in order of decreasing priority): (i) a Eurotherm Nanodac automatic data logger, (ii) a Zoom live stream of the meters (digitized with Google's Optical Character Recognition service), and (iii) real-time hand-recording and screenshots (of instantaneous rate only when the aircraft was directly overhead). The release point (stack coordinates 33.630637°, -114.487755°) was oriented vertically at height of 3.8m AGL.

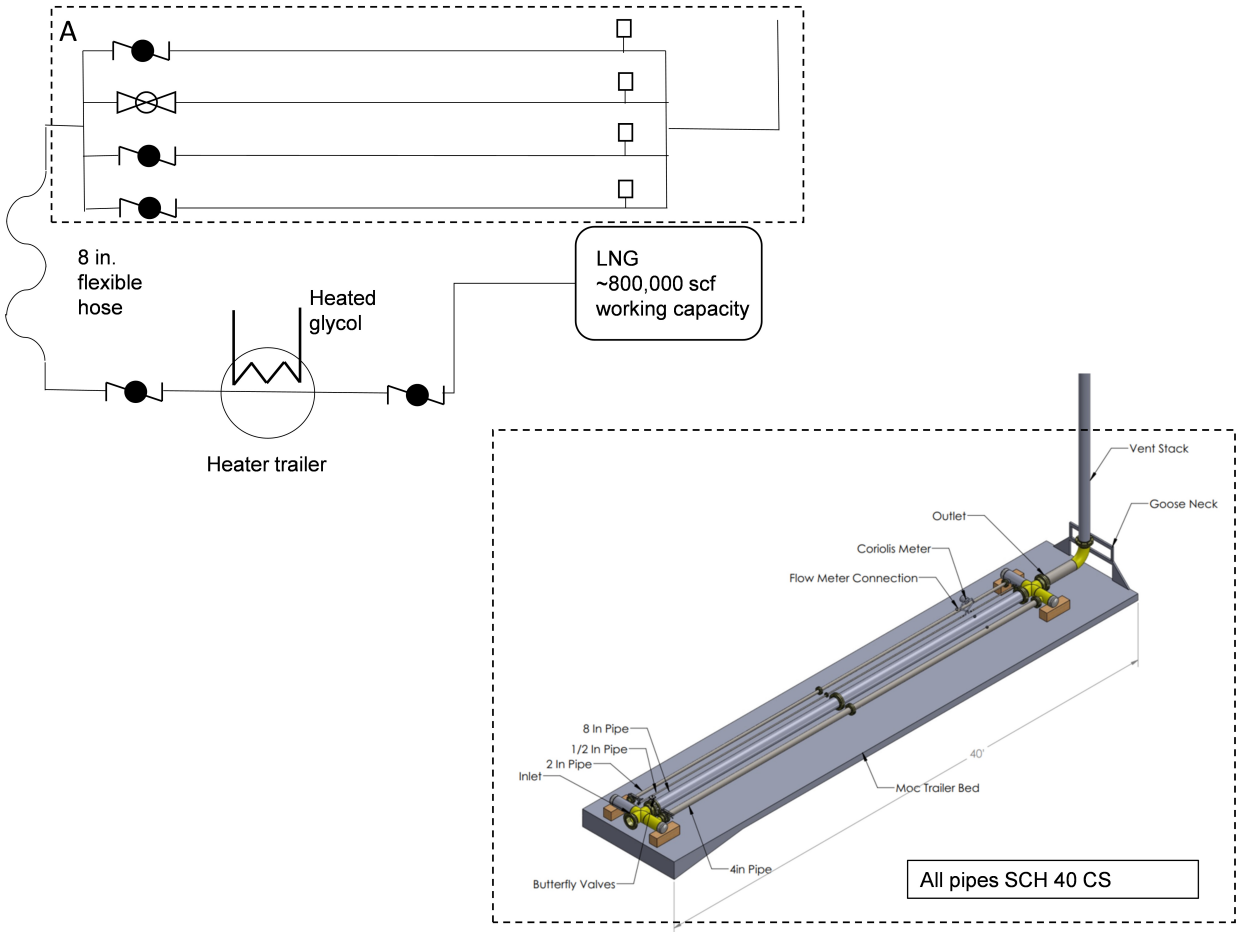

Figure 8. Schematic of release system in Ehrenberg, AZ.

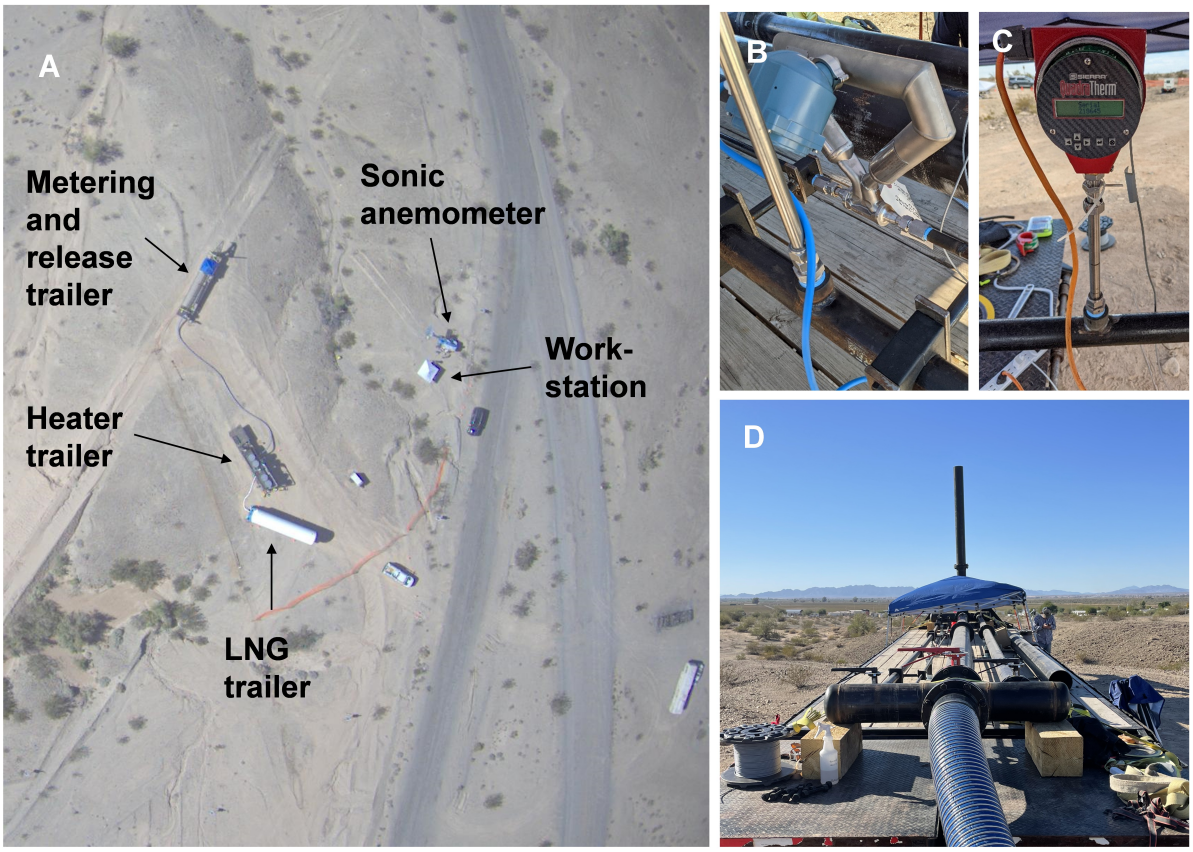

Figure 9. Photos of release system in Ehrenberg, AZ: U50 CNG trailer and control station (upper left), flow control and metering skid (lower left), and release point (right).)

Uncertainty of Metered Flow Rate in Midland, TX

We report the mean corrected methane flowrate with combined uncertainty as:

$$M_{CH_4} \pm \delta_{M_{CH_4}}$$

The mean methane flowrate,M_{CH_4}, is calculated as:

$$M_{CH_4} = Q_{CH_4} * \rho = \bar{Q} * \bar{X}_{CH_4} * \rho$$

where $\bar{Q}$ is the mean standard volumetric meter reading, $\bar{X}_{CH_4}$ is the mean methane mol fraction from gas analyses, and ρ is the density of methane at standard conditions.

Uncertainty in the mean methane flowrate, $\delta_{M_{CH_4}}$, includes:

1) Uncertainty in mean and flow meter reading,
2) Uncertainty in methane concentration

Uncertainty in mean and flow meter reading

The mean of the metered data is calculated as:

$$\bar{Q} = \frac{1}{n} * \sum_{1}^{n} Q_i = \frac{1}{n} * \sum_{1}^{n} (Q_m \pm \delta_m)$$

where Q_m is the meter reading and δ_m is the stated accuracy of the meter. δ_m can be factored out of the summation assuming the actual error introduced is the same for all measurements within the n measured values, a reasonable assumption for measurements of similar size:

$$\bar{Q} = \frac{1}{n} * \sum_{1}^{n} Q_m \pm \delta_m$$

The standard deviation is calculated as:

$$\sigma_Q = \sqrt{\frac{1}{n-1} \sum_{1}^{n} (Q_i - \bar{Q})^2}$$

Introducing the meter accuracy, the $\pm\delta_m$ term drops out, and therefore does not impact the standard deviation of the measurements:

$$\sigma_Q = \sqrt{\frac{1}{n-1} \sum_{1}^{n} (Q_m \pm \delta_m - (\bar{Q} \pm \delta_m))^2}$$

$$\sigma_Q = \sqrt{\frac{1}{n-1} \sum_{1}^{n} (Q_m \pm \delta_m - \bar{Q} \mp \delta_m)^2}$$

$$\sigma_Q = \sqrt{\frac{1}{n-1} \sum_{1}^{n} (Q_m - \bar{Q})^2}$$

Finally uncertainty in the mean is taken at $2\sigma_Q$:

$$Q = \bar{Q} \pm 2\sigma_Q \pm \delta_m$$

$$Q = \bar{Q} \pm (2\sigma_Q + \delta_m)$$

$$Q = \bar{Q} \pm \delta_Q$$

When evaluating the uncertainty the appropriate equation is applied from the respective flow meter calibration certificate.

1) Alicat 250 slpm: $\delta_m = \pm(0.8\%$ of reading +0.2% of full scale$)$
2) Alicat 5000 slpm: $\delta_m = \pm(0.8\%$ of reading +0.2% of full scale$)$

Uncertainty in methane mol fraction

Uncertainty in the methane mol fraction is calculated from n repeated gas composition analyses. The mean and standard deviation of X_{CH_4} is calculated as:

$$\bar{X}_{CH_4} = \frac{1}{n}\sum_{1}^{n} X_i$$

$$\sigma_X = \sqrt{\frac{1}{n-1}\sum_{1}^{n}(X_i - \bar{X}_{CH_4})^2}$$

Uncertainty in the mean is taken at $2\sigma_X$:

$$X = \bar{X} \pm \delta_X$$

$$X = \bar{X} \pm 2\sigma_X$$

Note, since only one composition analysis was performed for the Ehrenberg, AZ gas sample, the standard deviation and uncertainty in mol fraction is taken as zero. In the Midland, TX data the standard deviation of the methane mol fraction from the three repeated gas analyses is applied.

Combined uncertainty

The combined uncertainty in the mean volumetric methane flowrate, $\delta_{Q_{CH_4}}$, is calculated by quadrature propagation of uncertainty through the product $Q_{CH_4} = \bar{Q} * \bar{X}$ as:

$$\delta_{Q_{CH_4}} = Q_{CH_4}\sqrt{(\frac{\delta_Q}{\bar{Q}})^2 + (\frac{\delta_X}{\bar{X}})^2}$$

$$\delta_{Q_{CH_4}} = Q_{CH_4}\sqrt{(\frac{2(\sigma_Q + \frac{\delta_m}{2})}{\bar{Q}})^2 + (\frac{2\sigma_X}{\bar{X}})^2}$$

$$\delta_{Q_{CH_4}} = 2Q_{CH_4}\sqrt{(\frac{\sigma_Q}{\bar{Q}})^2 + (\frac{\sigma_Q\delta_m}{\bar{Q}^2}) + (\frac{\sigma_X}{\bar{X}})^2}$$

And uncertainty in the mass flow rate is taken as:

$$\delta_{M_{CH_4}} = \delta_{Q_{CH_4}} * \rho$$

Uncertainty of Metered Flow Rate in Ehrenberg, AZ

A modified approach is taken to quantifying uncertainty in release levels for the Stanford dataset. To accurately understand the accuracy of Quadratherm 640i in field conditions, a set of experiments were performed prior to the November 3-4 Bridger trials. A new Quadratherm 640i meter was purchased and a series of 18 meter comparison tests were performed between the new Quadratherm 640i and the Stanford set of older 640i meters (description of all three meters can be found in Rutherford et al. (2022). We classify two possible sources of error: (1) short-term noise that causes random variation in flow rate at time scales far shorter than a single experiment, and (2) long-term bias that persists as a consistent divergence between two meters that lasts for an entire experimental run. The Sierra-supplied error envelopes encompass the majority of the noise in the comparison trials (Sierra Instruments quotes the accuracy of the Quadratherm 640i as +/- 0.75% of reading with additional +/- 0.5% of full scale if below 50% of full scale). The comparison trials demonstrate that a bias of up to 6% between 640i meters can be observed. We believe this bias is likely due to mal-installation of the meter, even when installation is performed carefully. Thus, the Sierra supplied error envelopes accurately represent noise (short-term variance) in the Quadratherm 640i measurements, but do not account for bias due to other factors like meter mal-installation. The Stanford approach to quantifying error in Quadratherm 640i measurements is summarized as follows (with a more detailed description found in Rutherford et al. (2022)): (i) Adjust for possible systematic bias by randomly sampling from bias measurements observed in the comparison trials (nearly always between 0.95 and 1.05). (ii) Adjust for meter noise by using the Sierra error estimation method. (iii) Adjust for uncertainty in gas composition. In the Ehrenberg campaign, a weekly compositional analysis was performed by the supplier. The weekly compositional fractions of CH4 were 96.27%, 95.22% and 96.13% (all mole percent CH4). Because these compositions do not necessarily correspond to our cargos, we randomly sample from these with replacement. (iv) Finally, we add additional bias and noise terms for hand-recorded data only. Because hand-recorded data is at a lower resolution (approximately every 2.5 minutes) compared to secondly data for Nanodac or OCR-recorded data, the rolling average will under-represent variance.

Meter Calibrations

Calibration records for the Alicat mass flow controllers used in Midland, TX are shown in Figures 10 and 11. Records for the Sierra Quadratherm mass flow meter and the MicroMotion coriolis meter used in Ehrenberg, AZ are shown in Figures 12 and 13 respectively.

Certificate of Calibration

7641 N. Business Park Dr., Tucson, AZ 85743 U.S.A., 1.888.290.6060

ALICAT SCIENTIFIC

Device Under Test

Manufacturer:	Alicat Scientific, Inc.	**Control Algorithm:**	P=100 D=9000 I=0
Customer:	Bridger Photonics	**Software Version:**	9v03.0-R23
Sales Order:	SO370429	**Pressure Range:**	160.00 PSIA
Serial Number:	289497	**Pressure Accuracy:**	±0.5% of full scale
Model Number:	MCR-250SLPM-D	**Temperature Accuracy:**	±0.75°C
Adder Codes:	5M, 5IN, GAS: Air	**Standard Temp. & Pressure:**	25.00°C, 14.69595 PSIA
Range:	250.00 SLPM	**Normal Temp. & Pressure:**	0.00°C, 14.69595 PSIA
Process Gas:	Air (Selectable)	**Calibration Procedure:**	DOC-AUTOCAL-GASFLOW/Rev. 94
Calibration Gas:	Air	**Calibration Date:**	2021-09-08
Temperature:	28.23°C	**Certificate Number:**	362904
Humidity:	40%		

Equipment Used

All test equipment used for calibration is NIST traceable.

Type	Tool Name	Manufacturer/Model	Uncertainty	Due Date
Flow	TOOL-FLOW129	Alicat - MCRM-500SLPM	±0.32% reading or ±0.02% full scale, whichever is greater.	2022-08-21
Pressure	TOOL-PRESSURE21-145PSIG	Alicat - P-100PSIG-D	0.1% of reading	2021-12-09
Temperature	TOOL-TEMP15	ASL - F200-A-2+Probe	±0.02°C	2023-12-07
Voltage	TOOL-AIOC6	Alicat - AIOC	± 2.5mV and 4µA	2022-04-15

Calibration

Accuracy: ±0.8% of reading + ±0.2% of full scale.
Full Scale Range: 250.00 SLPM
Calibration Pressure: 64.67 PSIA

Valve Adjustment	
P1:	80 PSIG
P2:	0 PSIG

Output 1 Configuration
8-pin mini-DIN - Pin #6

Output 2 Configuration
8-pin mini-DIN - Pin #2

As-Left				
Indicated	**Actual**	**In Tolerance**	**Output 1**	**Output 2**
0.00	0.00	Yes	0.000 Vdc	5.120 Vdc
61.40	61.26	Yes	1.228 Vdc	5.120 Vdc
122.73	122.80	Yes	2.455 Vdc	5.120 Vdc
184.98	185.25	Yes	3.700 Vdc	5.120 Vdc
250.98	251.06	Yes	5.020 Vdc	5.120 Vdc

Error Chart

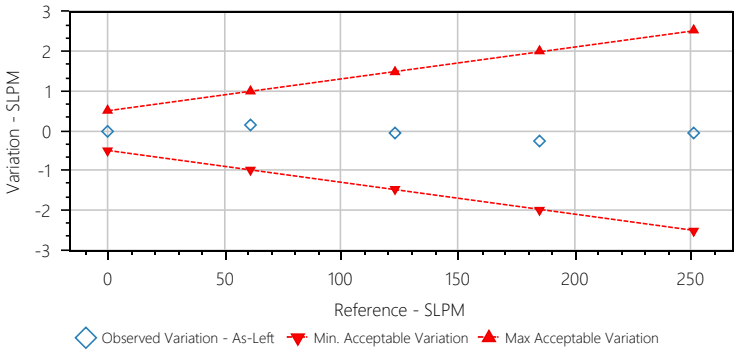

Control Response Chart

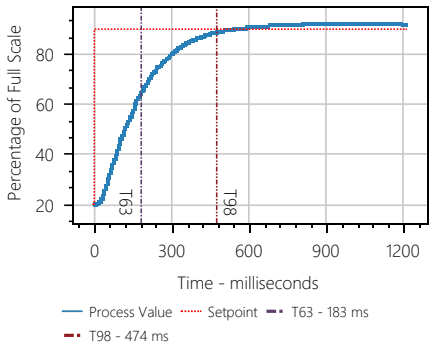

NOTES: Analog setpoint configured for 0-5Vdc.

Calibrated By: Ashlei Cota 2021-09-08 **QC Signature:**

Figure 10. Calibration certificate for 250 slpm Alicat mass flow controller.

Certificate of Calibration

7641 N. Business Park Dr., Tucson, AZ 85743 U.S.A., 1.888.290.6060

ALICAT SCIENTIFIC

Device Under Test

Manufacturer:	Alicat Scientific, Inc.	**Humidity:**	34%
Customer:	Bridger Photonics	**Control Algorithm:**	P=170 D=42500 I=0
Sales Order:	SO365689	**Software Version:**	8v31.0-R23
Serial Number:	270626	**Pressure Range:**	160.00 PSIA
Model Number:	MCRH-5000SLPM-D-PAR	**Pressure Accuracy:**	±0.5% of full scale
Adder Codes:	5M, 5IN, GAS: CH4, P1: 75 PSIG, P2: ATM, DS	**Temperature Accuracy:**	±0.75°C
Range:	5000.0 SLPM	**Standard Temp. & Pressure:**	25.00°C, 14.69595 PSIA
Process Gas:	CH4 (Selectable)	**Normal Temp. & Pressure:**	0.00°C, 14.69595 PSIA
Calibration Gas:	Air	**Calibration Procedure:**	DOC-AUTOCAL-GASFLOW/Rev. 94
Temperature:	26.94°C	**Certificate Number:**	335581

Equipment Used

All test equipment used for calibration is NIST traceable.

Type	Tool Name	Manufacturer/Model	Uncertainty	Due Date
Flow	TOOL-MOLBLOC14	Fluke Calibration - 1E4-S	± 0.2%	2022-08-13
Flow	TOOL-MOLBOX2	DH Instruments - Molbox 1 A...	NA \ Determined by Molbloc	2021-12-03
Pressure	TOOL-PRESSURE21-145PSIG	Alicat - P-100PSIG-D	0.1% of reading	2021-12-09
Temperature	TOOL-TEMP16	Alicat - N/A	± 0.2°C	2021-11-10
Voltage	TOOL-AIOC44	Alicat - AIOC	± 2.5mV and 4µA	2021-10-26

Calibration

Accuracy: ±0.8% of reading + ±0.2% of full scale.
Full Scale Range: 5000.0 SLPM
Calibration Pressure: 80.65 PSIA

Valve Adjustment	
P1:	75 PSIG
P2:	1 ATM

Output 1 Configuration
8-pin mini-DIN - Pin #6

Output 2 Configuration
8-pin mini-DIN - Pin #2

As-Left				
Indicated	**Actual**	**In Tolerance**	**Output 1**	**Output 2**
0.0	0.0	Yes	0.000 Vdc	5.120 Vdc
1249.6	1250.8	Yes	1.250 Vdc	5.120 Vdc
2500.3	2498.9	Yes	2.500 Vdc	5.120 Vdc
3751.0	3735.8	Yes	3.751 Vdc	5.120 Vdc
4999.7	4994.4	Yes	5.000 Vdc	5.120 Vdc

Error Chart

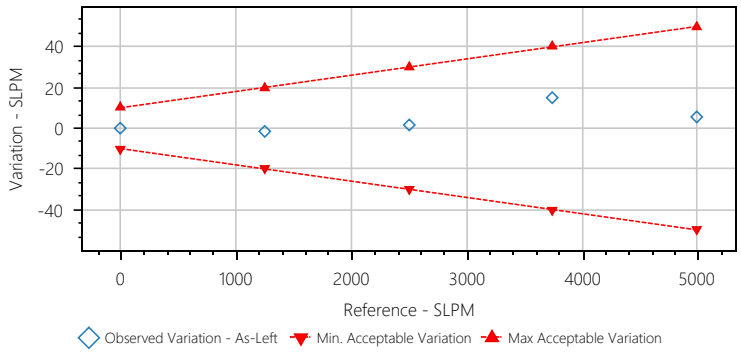

Control Response Chart

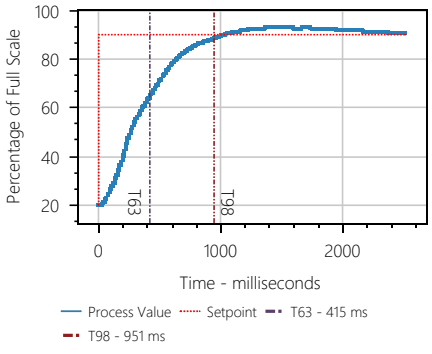

NOTES: Analog setpoint configured for 0-5Vdc.

Calibrated By: Benny Lopez 2021-02-03 **QC Signature:**

Figure 11. Calibration certificate for 5000 slpm Alicat mass flow controller.

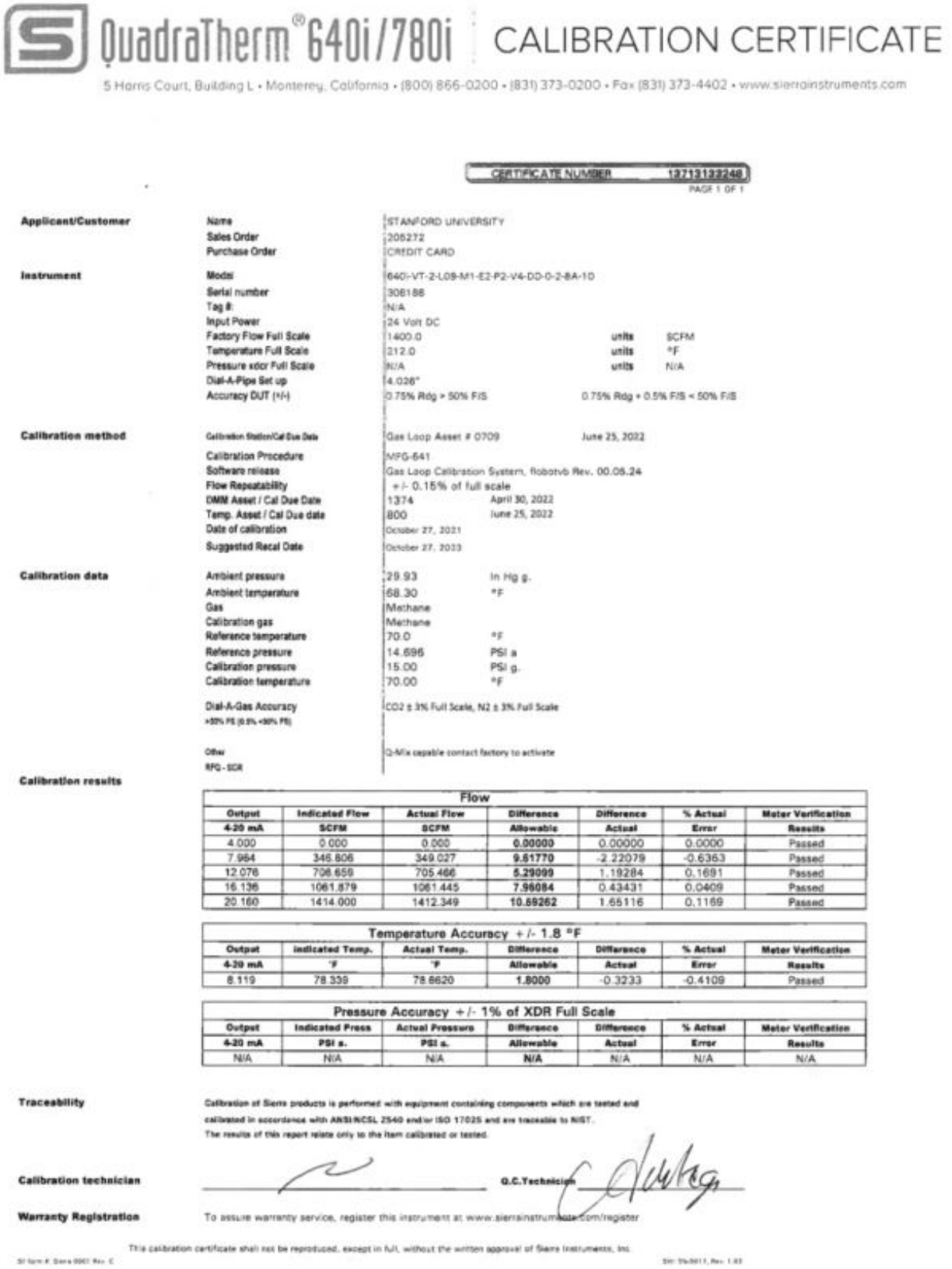

QuadraTherm® 640i/780i CALIBRATION CERTIFICATE

5 Harris Court, Building L • Monterey, California • (800) 866-0200 • (831) 373-0200 • Fax (831) 373-4402 • www.sierrainstruments.com

CERTIFICATE NUMBER 13713133248

PAGE 1 OF 1

Applicant/Customer

Name	STANFORD UNIVERSITY
Sales Order	205272
Purchase Order	CREDIT CARD

Instrument

Model	640i-VT-2-L09-M1-E2-P2-V4-DD-0-2-8A-1D		
Serial number	308188		
Tag #:	N/A		
Input Power	24 Volt DC		
Factory Flow Full Scale	1400.0	units	SCFM
Temperature Full Scale	212.0	units	°F
Pressure xdcr Full Scale	N/A	units	N/A
Dial-A-Pipe Set up	4.026"		
Accuracy DUT (+/-)	0.75% Rdg > 50% F/S	0.75% Rdg + 0.5% F/S < 50% F/S	

Calibration method

Calibration Station/Cal Due Date	Gas Loop Asset # 0709	June 25, 2022
Calibration Procedure	MPG-641	
Software release	Gas Loop Calibration System, Robotvb Rev. 00.06.24	
Flow Repeatability	+/- 0.15% of full scale	
DMM Asset / Cal Due Date	1374	April 30, 2022
Temp. Asset / Cal Due date	800	June 25, 2022
Date of calibration	October 27, 2021	
Suggested Recal Date	October 27, 2033	

Calibration data

Ambient pressure	29.93	In Hg g.
Ambient temperature	68.30	°F
Gas	Methane	
Calibration gas	Methane	
Reference temperature	70.0	°F
Reference pressure	14.696	PSI a
Calibration pressure	15.00	PSI g.
Calibration temperature	70.00	°F
Dial-A-Gas Accuracy (>50% FS (0.5% <50% FS)	CO2 ± 3% Full Scale, N2 ± 3% Full Scale	
Other	Q-Mix capable contact factory to activate	
RPG - SCR		

Calibration results

Flow

Output 4-20 mA	Indicated Flow SCFM	Actual Flow SCFM	Difference Allowable	Difference Actual	% Actual Error	Meter Verification Results
4.000	0.000	0.000	0.00000	0.00000	0.0000	Passed
7.964	346.806	349.027	9.81770	-2.22079	-0.6363	Passed
12.076	708.659	705.466	5.29099	1.19284	0.1691	Passed
16.136	1061.879	1061.445	7.96084	0.43431	0.0409	Passed
20.160	1414.000	1412.349	10.59262	1.65116	0.1169	Passed

Temperature Accuracy +/- 1.8 °F

Output 4-20 mA	Indicated Temp. °F	Actual Temp. °F	Difference Allowable	Difference Actual	% Actual Error	Meter Verification Results
8.119	78.339	78.6620	1.8000	-0.3233	-0.4109	Passed

Pressure Accuracy +/- 1% of XDR Full Scale

Output 4-20 mA	Indicated Press PSI a.	Actual Pressure PSI a.	Difference Allowable	Difference Actual	% Actual Error	Meter Verification Results
N/A	N/A	N/A	N/A	N/A	N/A	N/A

Traceability

Calibration of Sierra products is performed with equipment containing components which are tested and calibrated in accordance with ANSI/NCSL Z540 and/or ISO 17025 and are traceable to NIST. The results of this report relate only to the item calibrated or tested.

Calibration technician _____ **G.C.Technician** _____

Warranty Registration To assure warranty service, register this instrument at www.sierrainstruments.com/register

Figure 12. Calibration certificate for Quadratherm mass flow meter.

Micro Motion, Inc.

Mass Flowmeter Calibration Certificate

21175085

Product Code	Serial ID	Order ID	Line	Item	Customer Tag
CMF050M319N2BAEZZZ	21175085	10437147	1.1	1	
PUCK800	26169890				

Process

Process ID : 1.36412429
Process Time : 2021.09.21 21:11:37
Process Stand : TSM1C@SSCB:1
Stand Uncertainty : +/-0.030%
Fluid : H2O
100% Rate : 56.7 KG/MIN
Pickoff : 1
Max Rate P/T : 50.03 PSIG/22.7 C

Results

Status : PASS
D1 : 0
D2 : 1
K1 : 6366.231
K2 : 7630.057
DT : 4.5
FD : 342.6751
DTG : 0
DFQ1 : 0
DFQ2 : 0
FlowCal : 15.7464.29
FFQ : 0
FTG : 0
DensCal : 0636076304.50
FCF : 15.746
FT : 4.29

Detail

Flow (%)	Flow Rate (kg/min)	Meter Total (kg)	Reference Total (kg)	Error (%)	Specification (±%)
100.0	56.7	57.38985	57.39551	-0.010	0.100
10.0	5.67	5.649494	5.648243	0.022	0.100
50.0	28.35	27.98996	27.99243	-0.009	0.100
100.0	56.7	57.26417	57.26926	-0.009	0.100

BIJAY KHALING
Technician

This certificate is produced by an electronic data system and is valid without signature.

Traceable to one or more of the following National Metrology Institutes: NIM-China, NIST-USA, and VSL-The Netherlands

26.0.0.281 2021.09.21 21:28:41 1/1

Scanned with CamScanner

Figure 13. Calibration certificate for MicroMotion mass flow meter.

Gas Composition Analyses

Gas composition for the controlled release testing was assessed using a gas chromatograph. Three repeat analyses were performed on the gas sample from Midland, TX (Figures 14-16). One analysis was performed on the sample from Ehrenberg, AZ (Figure 17).

MITCHELL ANALYTICAL LABORATORY

2638 Faudree
Odessa, Texas 79765-8538
(432) 561-5579

Gas Analysis

Company:	Colorado State University		
Producer:	CSU	Sample Pressure:	55.0
Lease:	S2	Sample Temp:	90.0
Station #:	1	Date Sampled:	10/6/2021
Date Run:	10/11/2021	Sampled by:	CB
Lab Ref #:	21-OCT-103832	Field Gravity:	
Cylinder:		Field H2S:	0.0000
Analyzed by:	Blake		

Physical Constants per GPA 2145-09
All values calculated @ 60.0 Deg. F.

	Mole %	14.65 psia GPM (Ideal)	14.73 psia GPM (Ideal)	14.65 psia BTU (Ideal Dry)
Nitrogen	1.5851			0.000
CO2	0.4055			0.000
Methane	92.1636			930.900
Ethane	5.4318	1.444	1.453	96.100
Propane	0.4140	0.113	0.114	10.400
Iso-Butane	0.0000	0.000	0.000	0.000
N-Butane	0.0000	0.000	0.000	0.000
Iso-Pentane	0.0000	0.000	0.000	0.000
N-Pentane	0.0000	0.000	0.000	0.000
Hexanes +	0.0000	0.000	0.000	0.000
TOTALS	**100.0000**	**1.558**	**1.568**	**1034.200**

GROSS HEATING VALUE @ 14.65 psia

Dry	Wet	
1036	1020	BTU/Real Cu.Ft.
0.5958	0.5966	Specific Gravity (Real)
	1017	BTU/Ideal Cu.Ft.
0.5947		Specific Gravity (Ideal)
Z Factor :	0.9978	

GASOLINE CONTENT (GPM/Real)

Ethane and Heavier	1.5613
Propane and Heavie	0.1137
Butane and Heavier	0
Pentane and Heavie	0

Figure 14. Gas composition analysis from Midland TX, Sample 1.

MITCHELL ANALYTICAL LABORATORY

2638 Faudree
Odessa, Texas 79765-8538
(432) 561-5579

Gas Analysis

Company:	Colorado State University		
Producer:	CSU	Sample Pressure:	55.0
Lease:	S2	Sample Temp:	90.0
Station #:	2	Date Sampled:	10/6/2021
Date Run:	10/11/2021	Sampled by:	CB
Lab Ref #:	21-OCT-103833	Field Gravity:	
Cylinder:		Field H2S:	0.0000
Analyzed by:	Blake		

Physical Constants per GPA 2145-09
All values calculated @ 60.0 Deg. F.

	Mole %	14.65 psia GPM (Ideal)	14.73 psia GPM (Ideal)	14.65 psia BTU (Ideal Dry)
Nitrogen	1.5908			0.000
CO2	0.4060			0.000
Methane	92.1683			930.900
Ethane	5.4317	1.444	1.453	96.100
Propane	0.4032	0.110	0.111	10.100
Iso-Butane	0.0000	0.000	0.000	0.000
N-Butane	0.0000	0.000	0.000	0.000
Iso-Pentane	0.0000	0.000	0.000	0.000
N-Pentane	0.0000	0.000	0.000	0.000
Hexanes +	0.0000	0.000	0.000	0.000
TOTALS	**100.0000**	**1.555**	**1.565**	**1033.900**

GROSS HEATING VALUE @ 14.65 psia

Dry	Wet	
1036	1019	BTU/Real Cu.Ft.
0.5957	0.5965	Specific Gravity (Real)
	1017	BTU/Ideal Cu.Ft.
0.5946		Specific Gravity (Ideal)
Z Factor :	0.9978	

GASOLINE CONTENT (GPM/Real)

Ethane and Heavier	1.5583
Propane and Heavie	0.1107
Butane and Heavier	0
Pentane and Heavie	0

Figure 15. Gas composition analysis from Midland TX, Sample 2.

MITCHELL ANALYTICAL LABORATORY

2638 Faudree
Odessa, Texas 79765-8538
(432) 561-5579

Gas Analysis

Company:	Colorado State University		
Producer:	CSU	Sample Pressure:	55.0
Lease:	S2	Sample Temp:	90.0
Station #:	3	Date Sampled:	10/6/2021
Date Run:	10/11/2021	Sampled by:	CB
Lab Ref #:	21-OCT-103834	Field Gravity:	
Cylinder:		Field H2S:	0.0000
Analyzed by:	Blake		

Physical Constants per GPA 2145-09
All values calculated @ 60.0 Deg. F.

	Mole %	14.65 psia GPM (Ideal)	14.73 psia GPM (Ideal)	14.65 psia BTU (Ideal Dry)
Nitrogen	1.5797			0.000
CO2	0.4159			0.000
Methane	92.1614			930.800
Ethane	5.4385	1.446	1.455	96.200
Propane	0.4045	0.111	0.112	10.200
Iso-Butane	0.0000	0.000	0.000	0.000
N-Butane	0.0000	0.000	0.000	0.000
Iso-Pentane	0.0000	0.000	0.000	0.000
N-Pentane	0.0000	0.000	0.000	0.000
Hexanes +	0.0000	0.000	0.000	0.000
TOTALS	**100.0000**	**1.557**	**1.567**	**1034.000**

GROSS HEATING VALUE @ 14.65 psia

Dry	Wet	
1036	1019	BTU/Real Cu.Ft.
0.5958	0.5966	Specific Gravity (Real)
	1017	BTU/Ideal Cu.Ft.
0.5947		Specific Gravity (Ideal)
Z Factor :	0.9978	

GASOLINE CONTENT (GPM/Real)

Ethane and Heavier	1.5604
Propane and Heavie	0.1111
Butane and Heavier	0
Pentane and Heavie	0

Figure 16. Gas composition analysis from Midland TX, Sample 3.

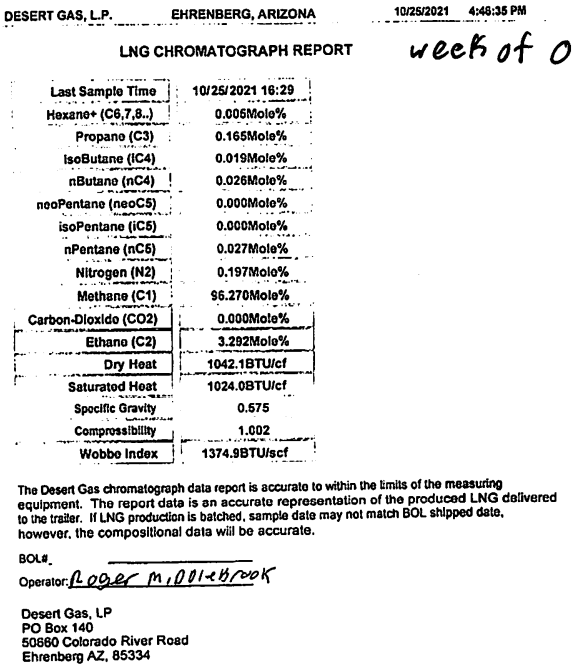

DESERT GAS, L.P. EHRENBERG, ARIZONA 10/25/2021 4:48:35 PM

LNG CHROMATOGRAPH REPORT week of Oct 24th - 30th

Last Sample Time	10/25/2021 16:29
Hexane+ (C6,7,8..)	0.005Mole%
Propane (C3)	0.165Mole%
IsoButane (IC4)	0.019Mole%
nButane (nC4)	0.026Mole%
neoPentane (neoC5)	0.000Mole%
isoPentane (iC5)	0.000Mole%
nPentane (nC5)	0.027Mole%
Nitrogen (N2)	0.197Mole%
Methane (C1)	96.270Mole%
Carbon-Dioxide (CO2)	0.000Mole%
Ethane (C2)	3.292Mole%
Dry Heat	1042.1BTU/cf
Saturated Heat	1024.0BTU/cf
Specific Gravity	0.575
Compressibility	1.002
Wobbe Index	1374.9BTU/scf

The Desert Gas chromatograph data report is accurate to within the limits of the measuring equipment. The report data is an accurate representation of the produced LNG delivered to the trailer. If LNG production is batched, sample date may not match BOL shipped date, however, the compositional data will be accurate.

BOL#

Operator: Roger Middlebrook

Desert Gas, LP
PO Box 140
50860 Colorado River Road
Ehrenberg AZ, 85334

Figure 17. Gas composition analysis from Ehrenberg AZ, Sample 1.

Controlled Release Demographics

Controlled release testing included 650 individual measurement passes. Testing was conducted at two nominal flight altitudes to evaluate the detection limits at each (Figure 18). Testing in Ehrenberg, AZ only included flights at nominal altitude of 675' AGL. The average windspeed (10m AGL) during a single pass ranged from 0.48 m/s to 7.99 m/s (Figure 19).

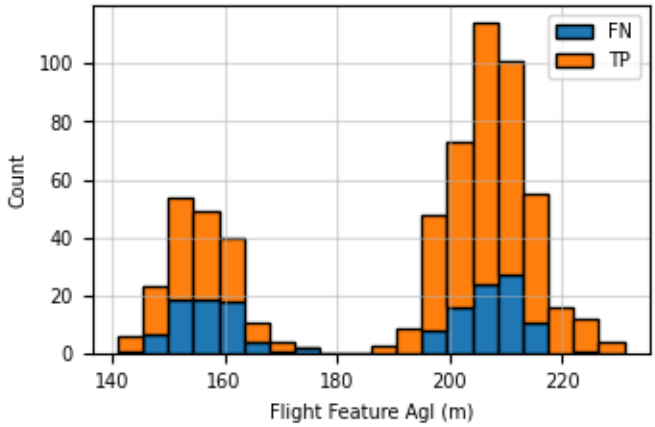

Figure 18. Histogram of flight altitude on each measurement pass. Stacked bars show true positive and false negative results. Passes where the plume was not established are excluded from the figure. Passes below 180 m were considered a nominal flight altitude of 500' AGL and passes above 180m were considered a nominal flight altitude of 675' AGL.

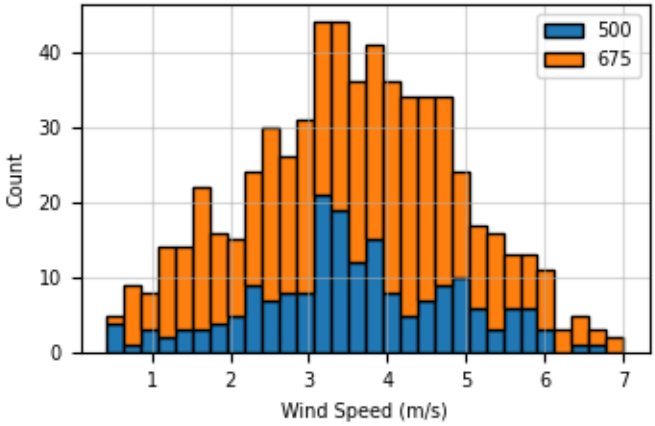

Figure 19. Histogram of windspeed on each measurement pass. Stacked bars show nominal altitudes of each pass. Passes where the plume was not established are excluded from the figure.

Detection Curves

Detection curves are shown for wind speeds of 0-2 m/s, 2-4 m/s, and 4-6 m/s in Figures 20 through 22 respectively for nominal flight altitude of 500' AGL, and in Figures 23-25 for nominal altitude of 675' AGL. These curves are produced by filtering data to the respective range of wind conditions and applying the same binomial regression (logit) technique as utilized for the wind-normalized detection results in the main paper. Separate curves derived from the wind-normalized result are also shown in each figure for the lower bound, upper bound, and mean wind speed of the represented data. Note, filtering to a subset of wind conditions and altitude results in a reduced sample size relative to the full dataset, and therefore generally result in wider uncertainty and lower statistical power. However, the curves derived from the wind-normalized emission rate detection curve agree well with the wind-filtered emission rate curves: The curves developed by scaling the normalized result using the mean wind speed for each subset (red dotted line) agree closely with the regression to the subset itself (blue solid line). Additionally, the curves developed by scaling the normalized result using the lower and upper wind speed (red dash-dot and dashed lines respectively) reflect the lower and upper confidence illustrated by the bootstrapped results.

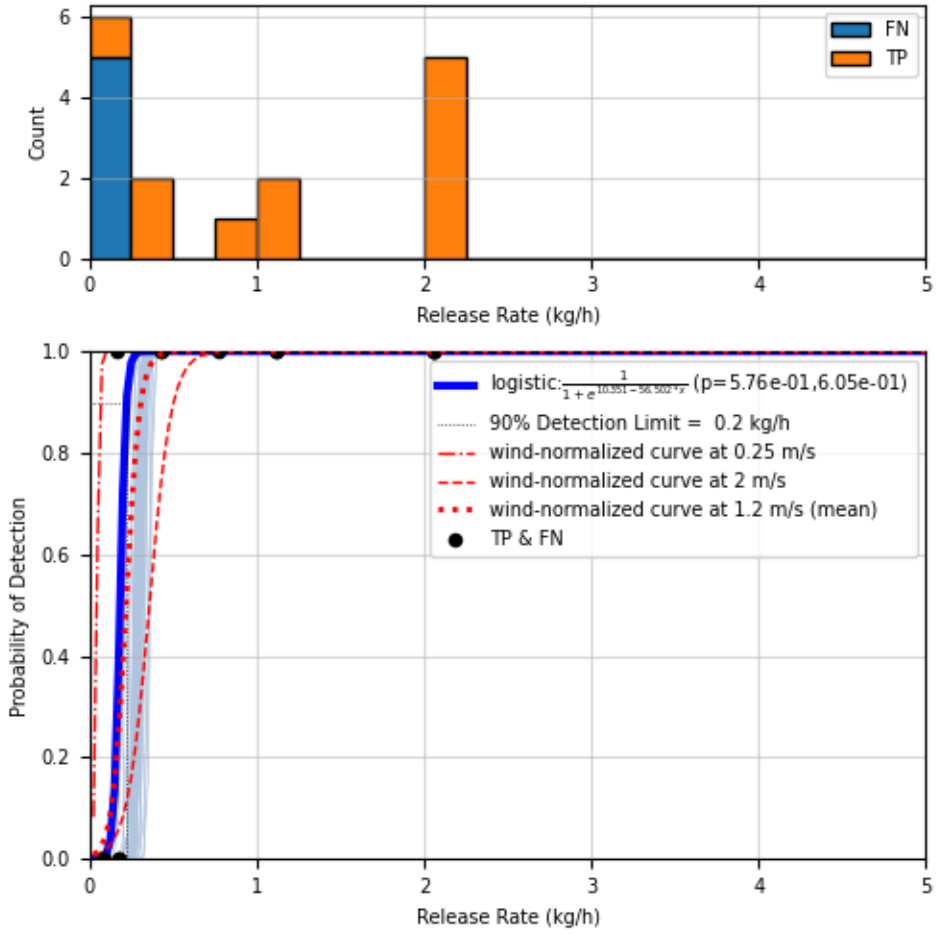

Figure 20. Detection sensitivity at 500' AGL nominal flight altitude and 0-2 m/s windspeed. A histogram in the upper panel shows the count of true positive and false negative detections underlying the binomial regression shown in the lower panel. True positive and false negative data points are shown at y = 1 and y = 0 respectively. Bootstrapping is used to resample from the data and repeat the regression to show the confidence bounds of the result. A 90.0% detection rate is observed at 0.2 kg/h. Curves derived from the wind-normalized regression at fixed wind speeds corresponding to the lower edge, upper edge, and mean of the filtered data are shown in red.

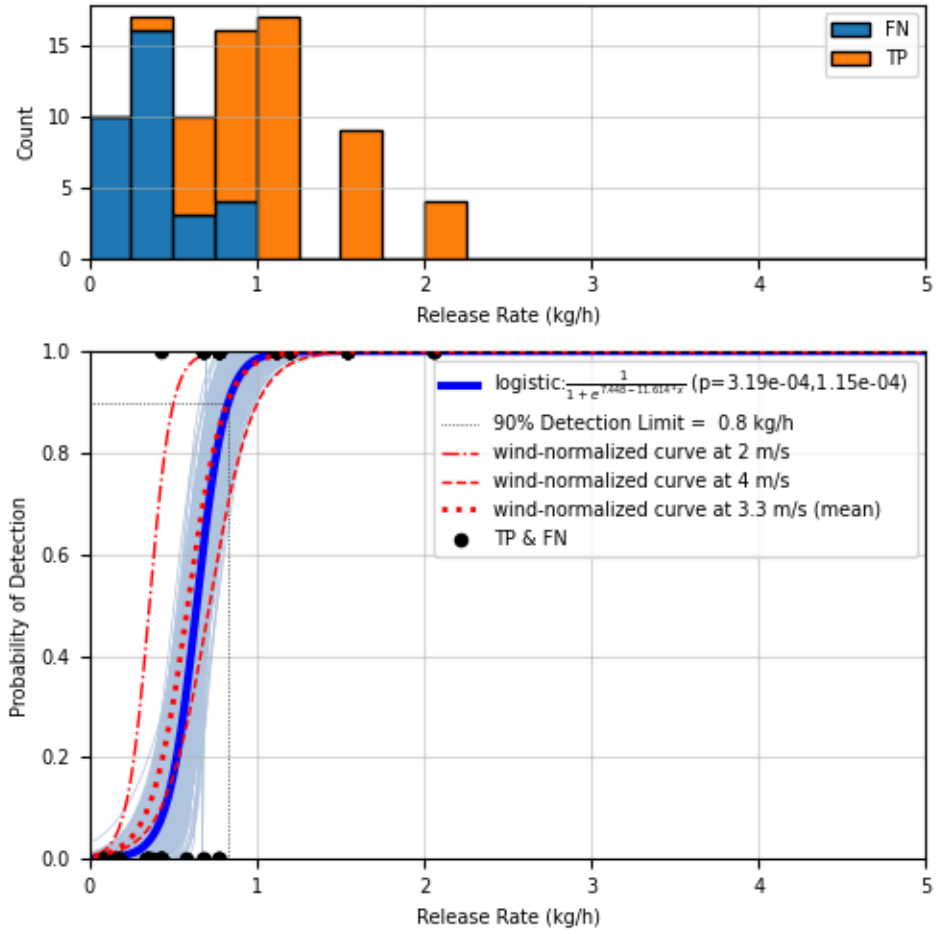

Figure 21. Detection sensitivity at 500' AGL nominal flight altitude and 2-4 m/s windspeed. A histogram in the upper panel shows the count of true positive and false negative detections underlying the binomial regression shown in the lower panel. True positive and false negative data points are shown at y = 1 and y = 0 respectively. Bootstrapping is used to resample from the data and repeat the regression to show the confidence bounds of the result. A 90.0% detection rate is observed at 0.8 kg/h. Curves derived from the wind-normalized regression at fixed wind speeds corresponding to the lower edge, upper edge, and mean of the filtered data are shown in red.

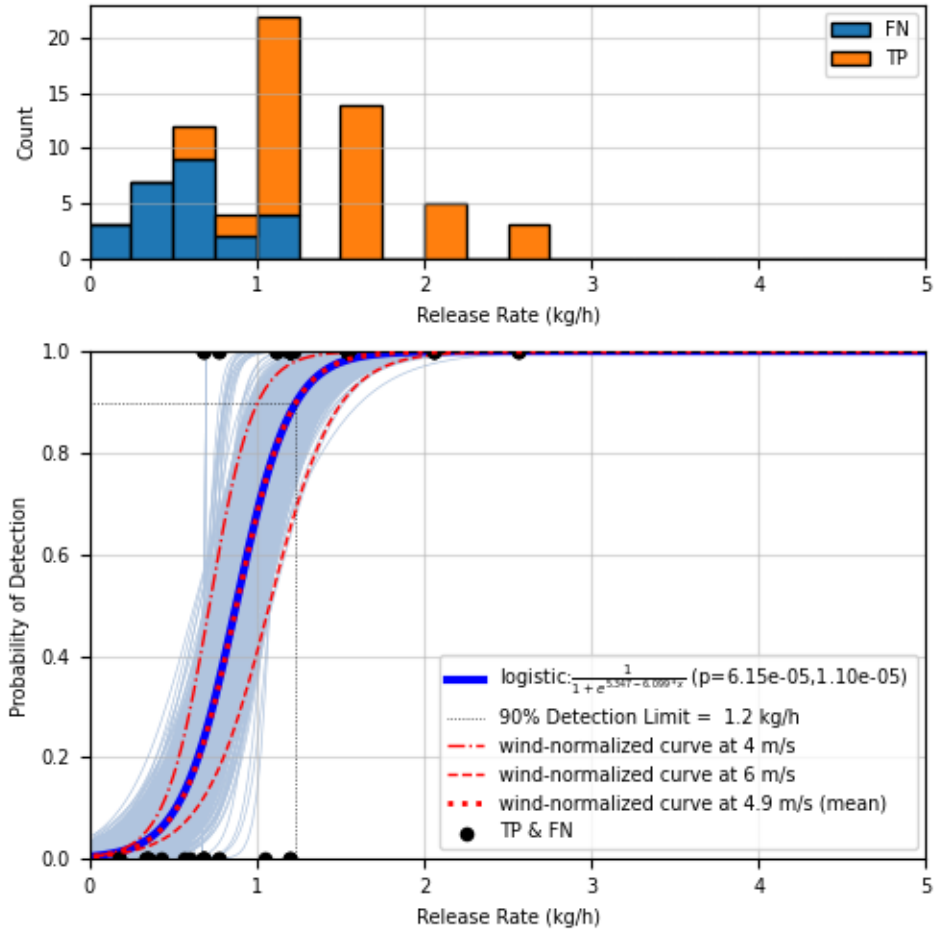

Figure 22. Detection sensitivity at 500' AGL nominal flight altitude and 4-6 m/s windspeed. A histogram in the upper panel shows the count of true positive and false negative detections underlying the binomial regression shown in the lower panel. True positive and false negative data points are shown at y = 1 and y = 0 respectively. Bootstrapping is used to resample from the data and repeat the regression to show the confidence bounds of the result. A 90.0% detection rate is observed at 1.2 kg/h. Curves derived from the wind-normalized regression at fixed wind speeds corresponding to the lower edge, upper edge, and mean of the filtered data are shown in red.

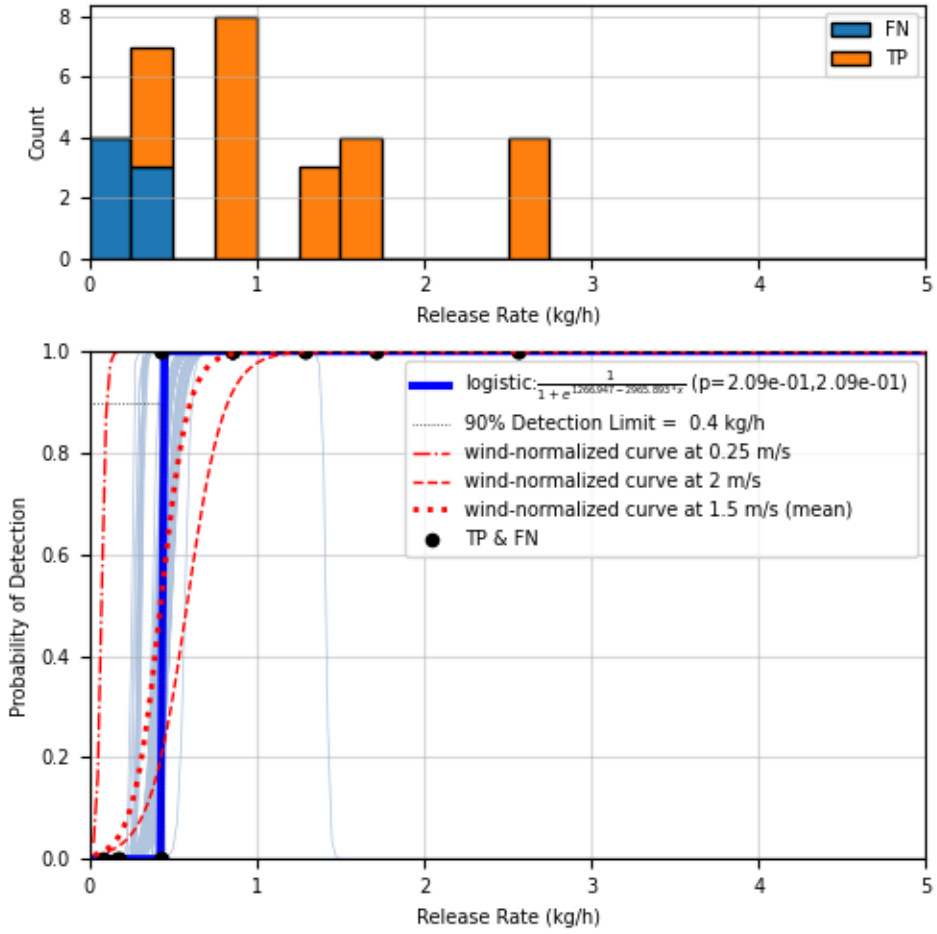

Figure 23. Detection sensitivity at 675' AGL nominal flight altitude and 0-2 m/s windspeed. A histogram in the upper panel shows the count of true positive and false negative detections underlying the binomial regression shown in the lower panel. True positive and false negative data points are shown at y = 1 and y = 0 respectively. Bootstrapping is used to resample from the data and repeat the regression to show the confidence bounds of the result. A 90.0% detection rate is observed at 0.4 kg/h. Curves derived from the wind-normalized regression at fixed wind speeds corresponding to the lower edge, upper edge, and mean of the filtered data are shown in red.

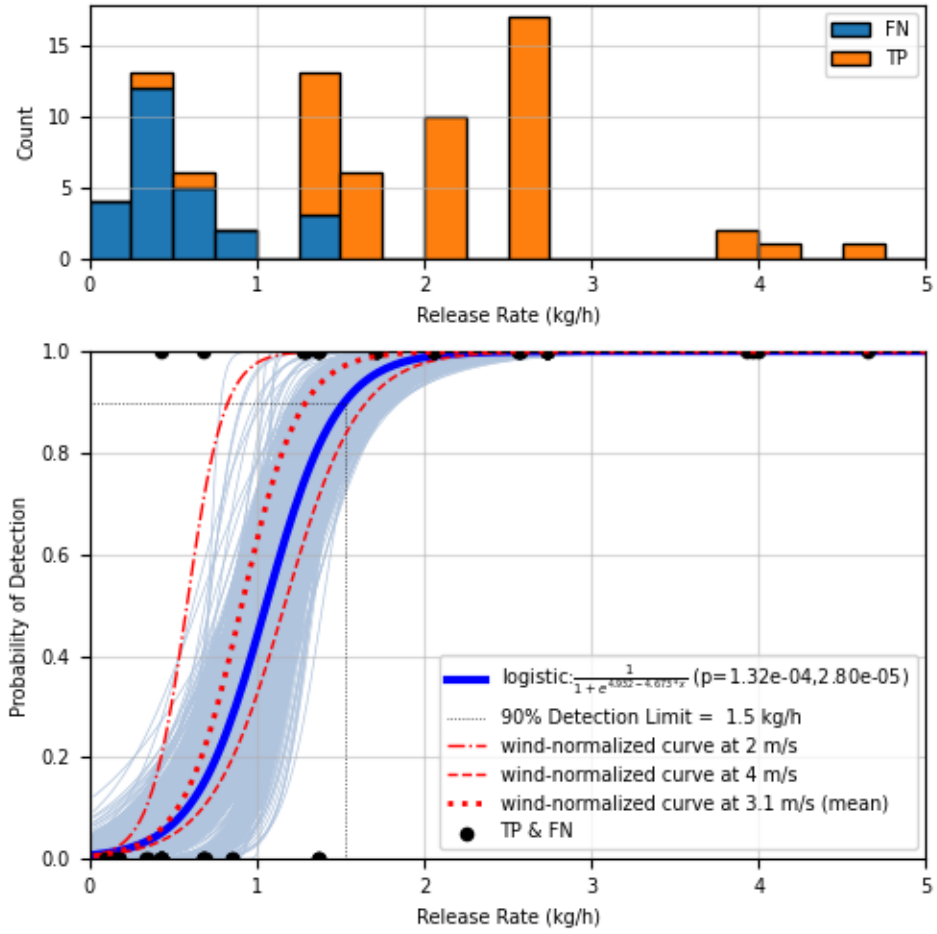

Figure 24. Detection sensitivity at 675' AGL nominal flight altitude and 2-4 m/s windspeed. A histogram in the upper panel shows the count of true positive and false negative detections underlying the binomial regression shown in the lower panel. True positive and false negative data points are shown at y = 1 and y = 0 respectively. Bootstrapping is used to resample from the data and repeat the regression to show the confidence bounds of the result. A 90.0% detection rate is observed at 1.5 kg/h. Curves derived from the wind-normalized regression at fixed wind speeds corresponding to the lower edge, upper edge, and mean of the filtered data are shown in red.

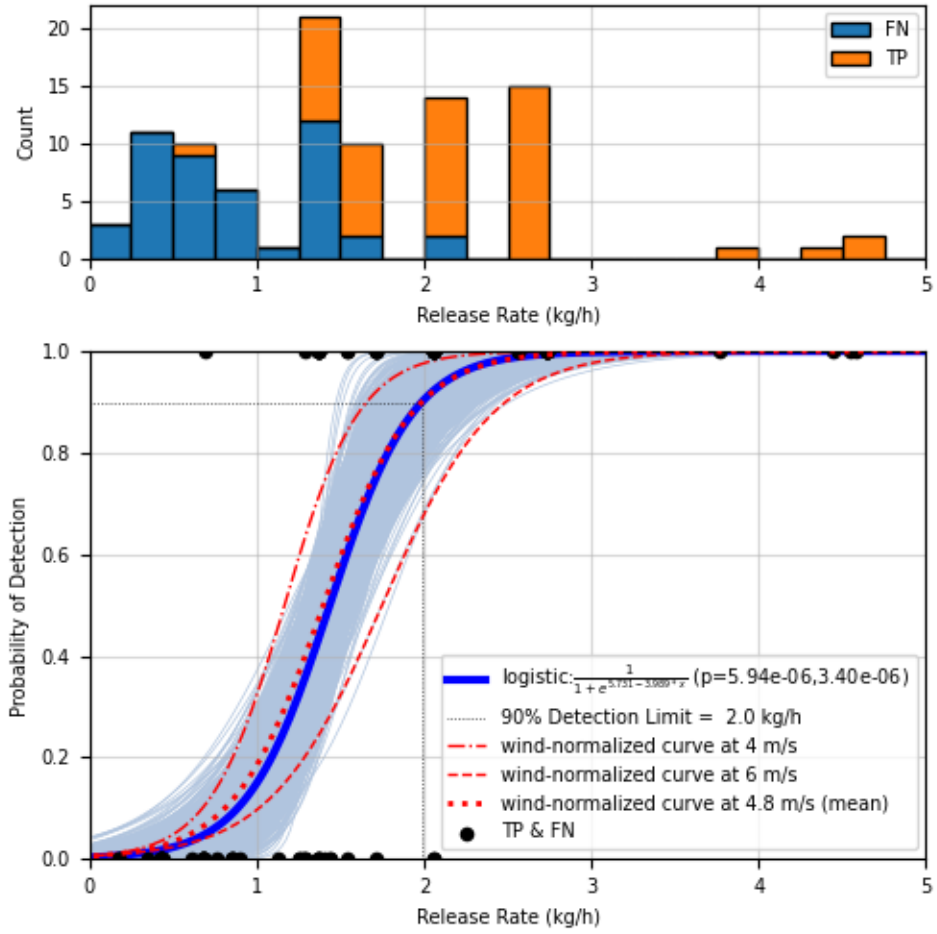

Figure 25. Detection sensitivity at 675' AGL nominal flight altitude and 4-6 m/s windspeed. A histogram in the upper panel shows the count of true positive and false negative detections underlying the binomial regression shown in the lower panel. True positive and false negative data points are shown at y = 1 and y = 0 respectively. Bootstrapping is used to resample from the data and repeat the regression to show the confidence bounds of the result. A 90.0% detection rate is observed at 2.0 kg/h. Curves derived from the wind-normalized regression at fixed wind speeds corresponding to the lower edge, upper edge, and mean of the filtered data are shown in red.

Quantification Accuracy

Since a higher fractional error was observed at low emission rates and low wind speeds in the HRRR dataset, the quantification analysis was repeated with these data excluded (Figure 26). This resulted in the exclusion of 270 data points where 10m windspeed was below 2m/s or the controlled release rate was below 3 kg/h. The regression result shows these higher error regions have little impact on the linear regression (upper subplot) when compared to the regression performed on the full dataset.

The quantification analysis was repeated for each of the three wind data sources (HRRR, NAM12, and local sonic anemometer). Figures 27 - 30 show the results for the NAM12 and sonic datasets. The NAM12 wind results in a regression with a low bias, and a similar case can be seen as in the HRRR data, where low emission rates and low wind speeds tend to increase the error of measurements. The sonic wind results in a regression with a high bias. The data exhibit a similar result at low emission rates, however the sonic data improves the measurement accuracy under low wind conditions. Distribution of measurement errors are shown in Figure 31 for each wind data source.

The wind velocity used in Bridger's emission rate estimate is an estimate at the plume height, interpolated from the 10m modeled (HRRR or NAM12) wind field. This data is reported in the dataset as *Detection Wind Speed (mph)*. The 10m wind speed used by Bridger is also reported as Wind Speed 10m (mph). Because the anemometers were installed at fixed heights, the wind speed at the plume height was not measured directly. In the case of the Ehrinberg data, the wind speed was measured at 10m AGL, and can be compared directly to the 10m HRRR and NAM12 estimate from Bridger during each pass. In Midland it was not feasible to set the anemometers at 10m AGL, so 10m winds are estimated by extrapolating from the measured height. We calculate and report a wind speed at the same plume height for each pass based on our anemometer data, *cr WindSpeedAtPlumeHeight mps*, and an error estimate *Error WindSpeedAtPlumeHeight percent*. In Figure 32 the wind difference in the emission rate estimate is plotted versus the difference in wind speed at the plume height, both in percent error, for each wind technique (HRRR, NAM12, and with our sonic). Visual inspection of the data shows positive correlation where when the wind speed is underestimated the resulting emission rate is underestimated, and when the wind speed is overestimated, the resulting emission rate is over estimated. However this is not always the case and there is a significant amount of datapoints in all four quadrants (++, +-, –, and -+ error in wind and error in emission rate respectively). Note, it would be expected that when the sonic data was provided, the points should all collapse to 0 on the x-axis (fall into a vertical line), however this does not happen (x-error improves but still non zero). This is due to differences in time averaging methodologies used by Bridger and the study team (i.e. Bridger averages over the *Flight Feature Time*, while the study team averaged wind over a fixed time frame preceeding each *Detection Time* as described in the paper).

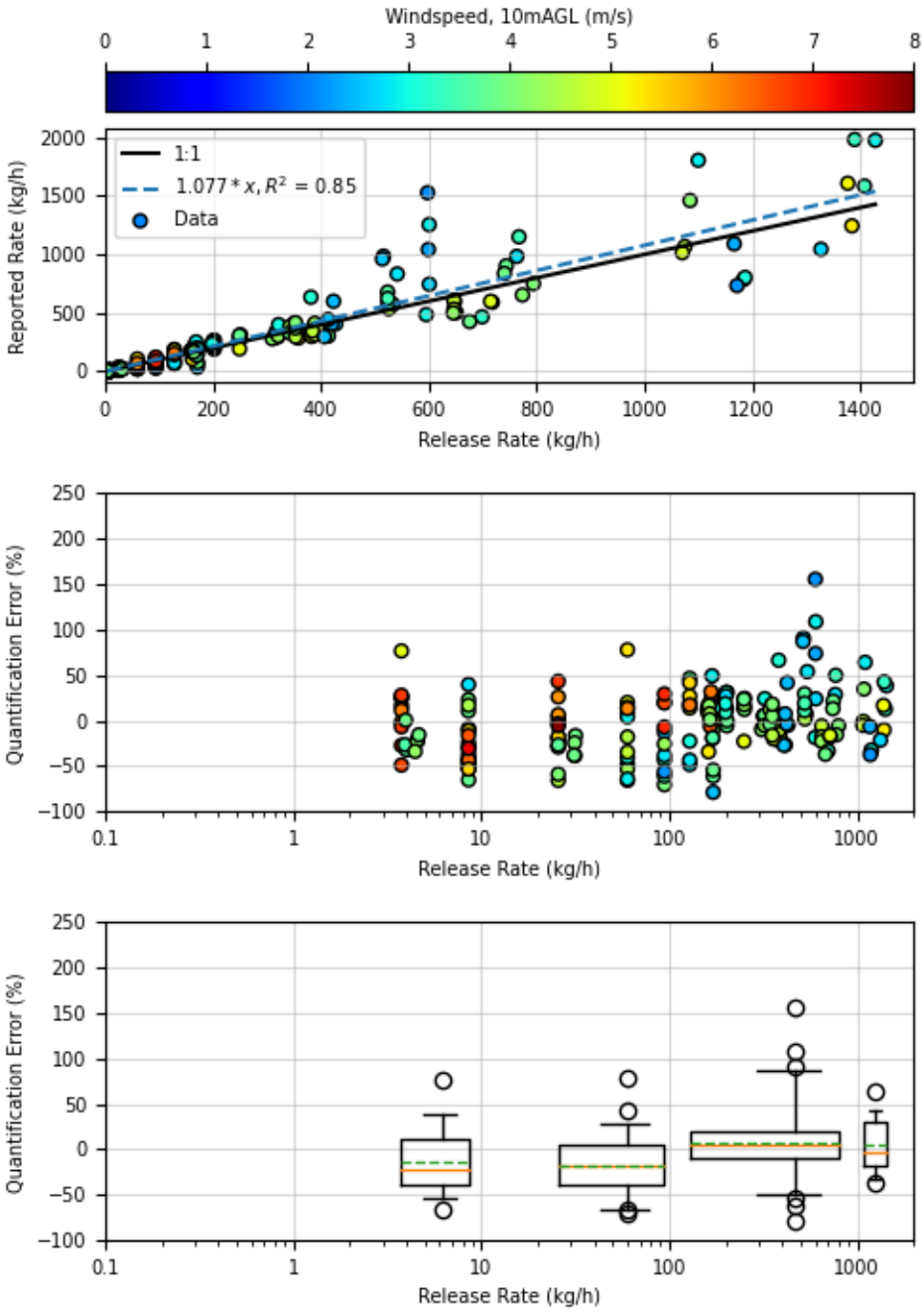

Figure 26. Accuracy of emission estimates produced with HRRR data vs release rate, excluding data where wind speed was less than 2m/s or emission rate was less than 3 kg/h. Linear regression with no intercept (Measured = 1.081*Metered) indicates a bias of 8.1% high across the data (upper panel). Error of individual measurements are shown as a percentage of the metered release rate (center panel). Marker colors represent the average windspeed preceeding the measurement. A box and whisker plot (lower panel) illustrates the mean (dashed line), median (solid line), inner quartiles (box), and 95% confidence (whiskers) for data within each order of magnitude. Fliers are shown for data outside the 95% CI of each boxplot. Note, the y-limits of the center and bottom panels are set to a maximum of 250% error to correspond to axis limits of other comparable figures, although 0 data points exceed 250% error in this subset. Only true positive detections are included in the figures and regression.

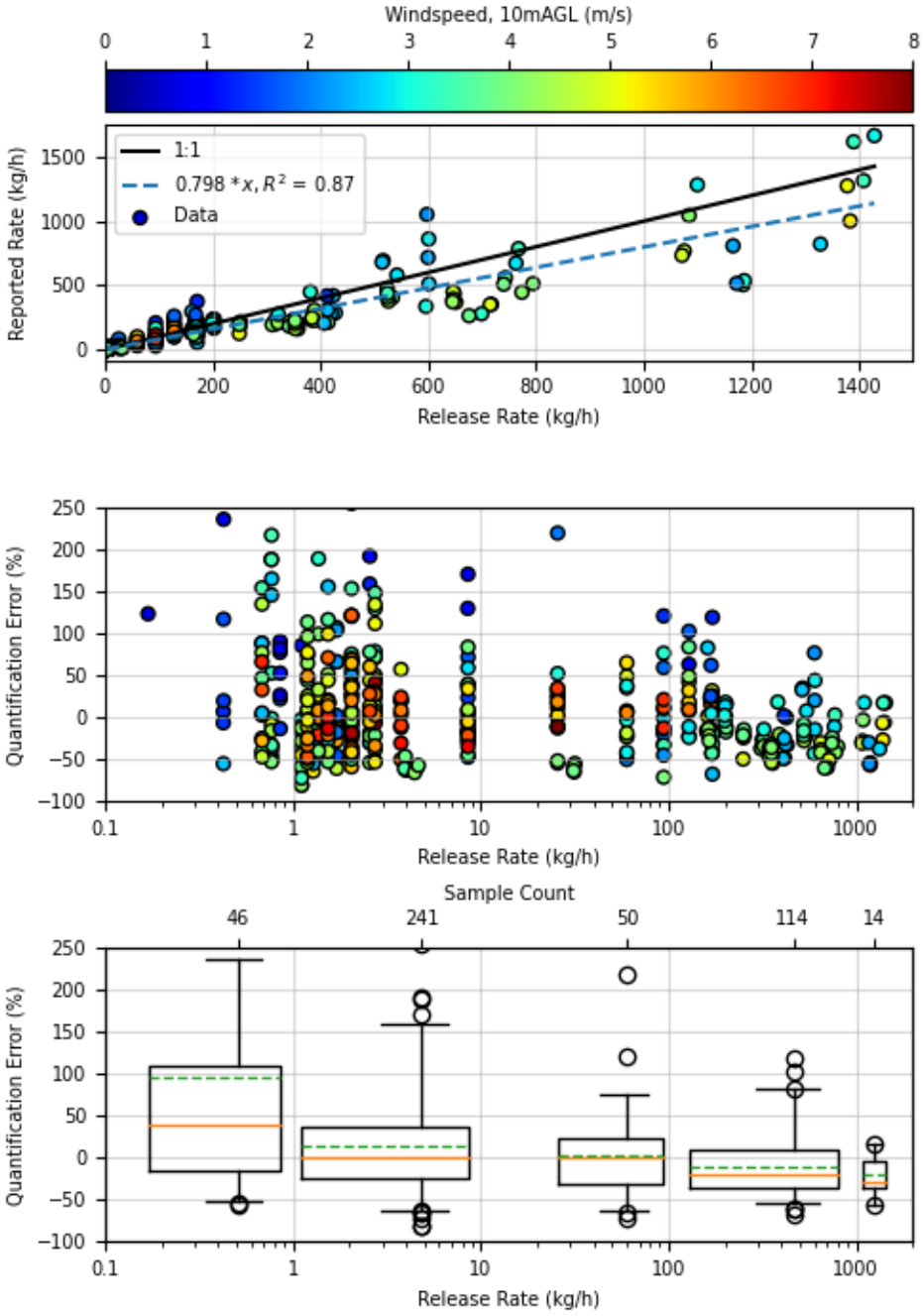

Figure 27. Accuracy of emission estimates produced with NAM12 data vs release rate. Linear regression with no intercept (Measured = 0.798*Metered) indicates a bias of -20.2% low across the data (upper panel). Error of individual measurements are shown as a percentage of the metered release rate (center panel). Marker colors represent the average windspeed preceeding the measurement. A box and whisker plot (lower panel) illustrates the mean (dashed line), median (solid line), inner quartiles (box), and 95% confidence (whiskers) for data within each order of magnitude. Fliers are shown for data outside the 95% CI of each boxplot. Note, the y-limits of the center and bottom panels are set to a maximum of 250% error to improve visibility of the figures although 5 data points exceed 250% error. Only true positive detections are included in the figures and regression.

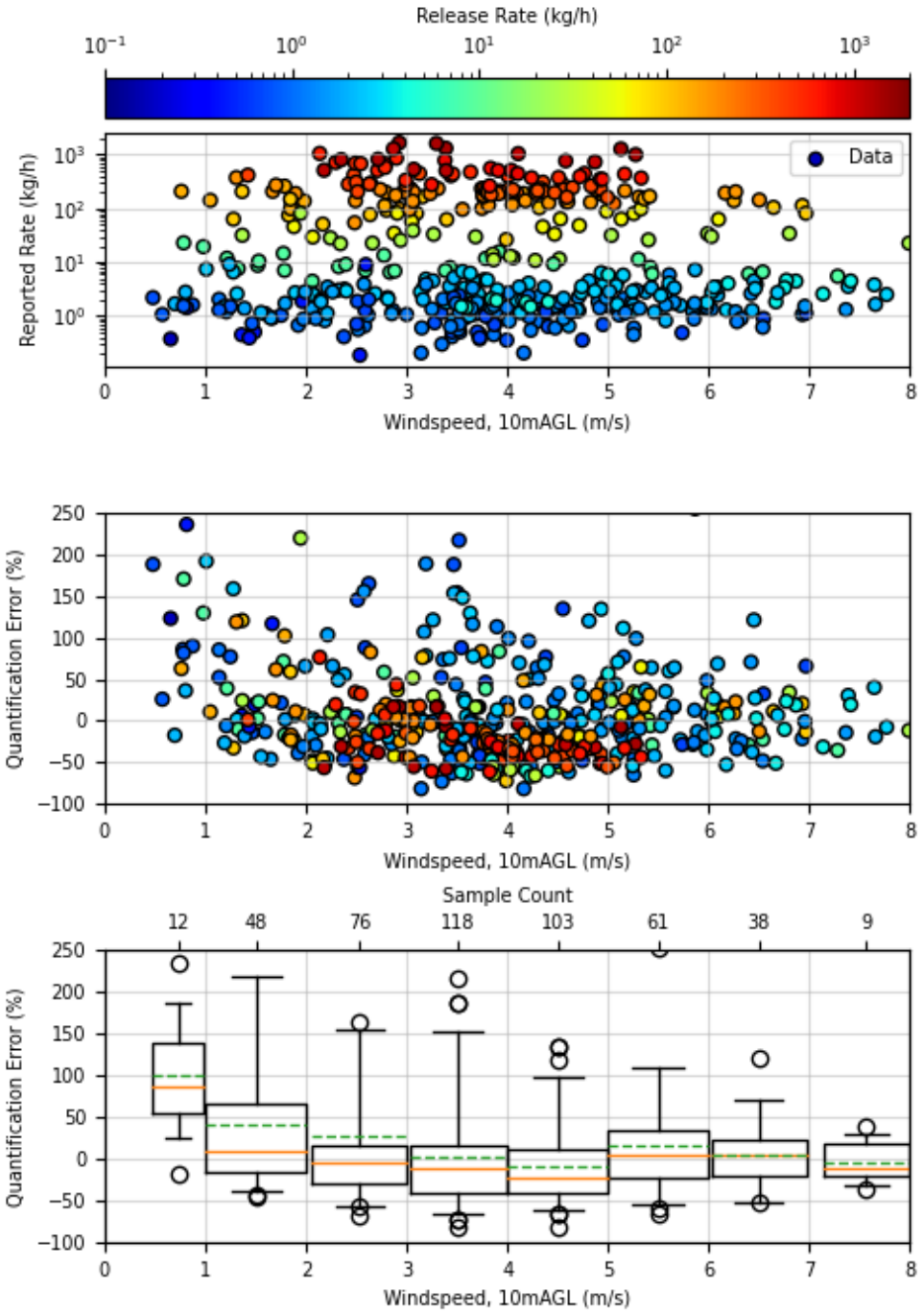

Figure 28. Accuracy of emission estimates produced with NAM12 data vs windspeed. Marker colors represent the release rate. Error of individual measurements are shown as a percentage of the metered release rate (center panel). A box and whisker plot (lower panel) illustrates the mean (dashed line), median (solid line), inner quartiles (box), and 95% confidence (whisker) for data within each m/s wind category. Note, the y-limits of the center and bottom panels are set to a maximum of 250% error to improve visibility of the figures although 5 data points exceed 250% error. Only true positive detections are included in the figures and regression.

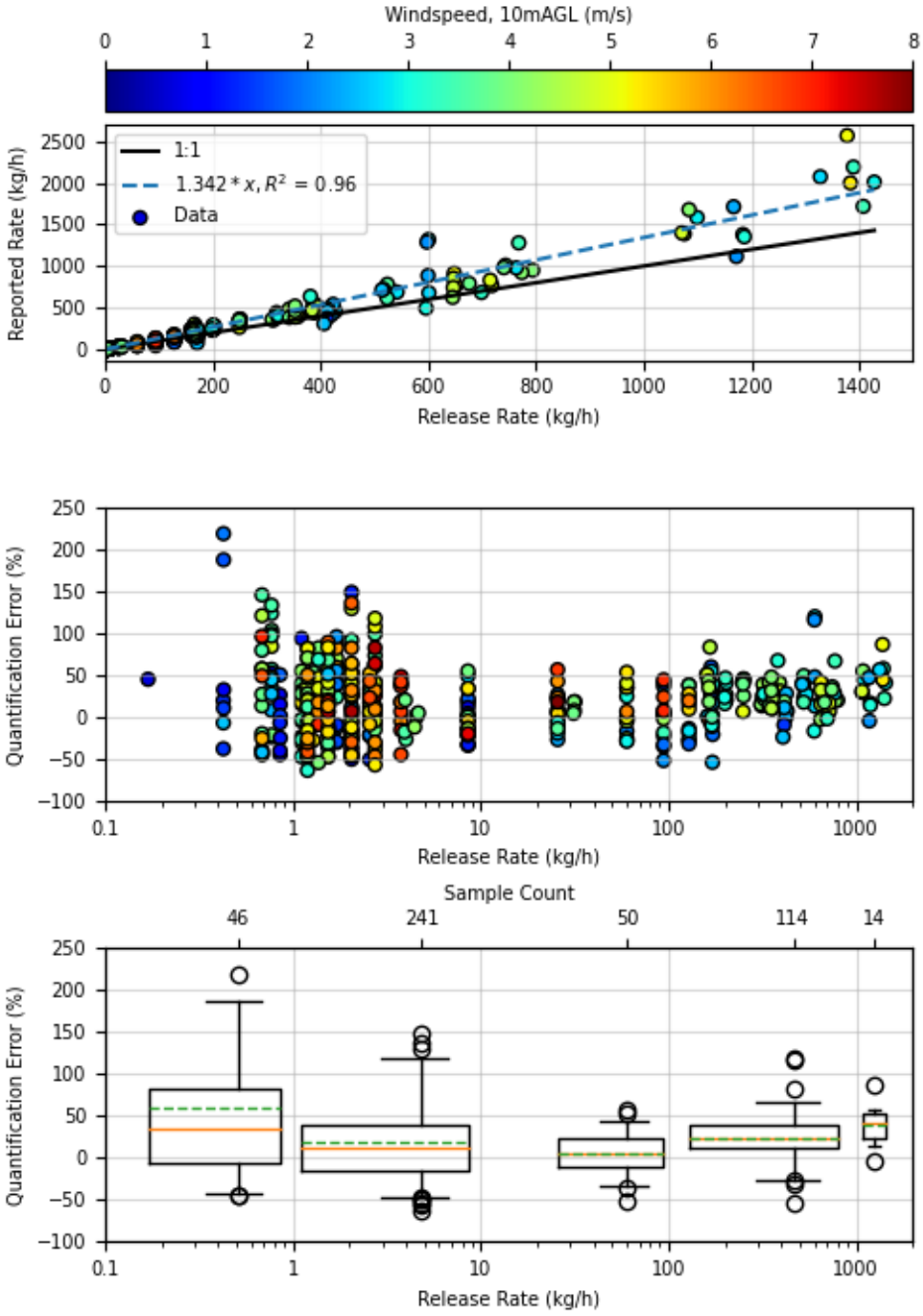

Figure 29. Accuracy of emission estimates produced with sonic data vs release rate. Linear regression with no intercept (Measured = 1.342*Metered) indicates a bias of 34.2% high across the data (upper panel). Error of individual measurements are shown as a percentage of the metered release rate (center panel). Marker colors represent the average windspeed preceeding the measurement. A box and whisker plot (lower panel) illustrates the mean (dashed line), median (solid line), inner quartiles (box), and 95% confidence (whiskers) for data within each order of magnitude. Fliers are shown for data outside the 95% CI of each boxplot. Note, the y-limits of the center and bottom panels are set to a maximum of 250% error to improve visibility of the figures although 4 data points exceed 250% error. Only true positive detections are included in the figures and regression.

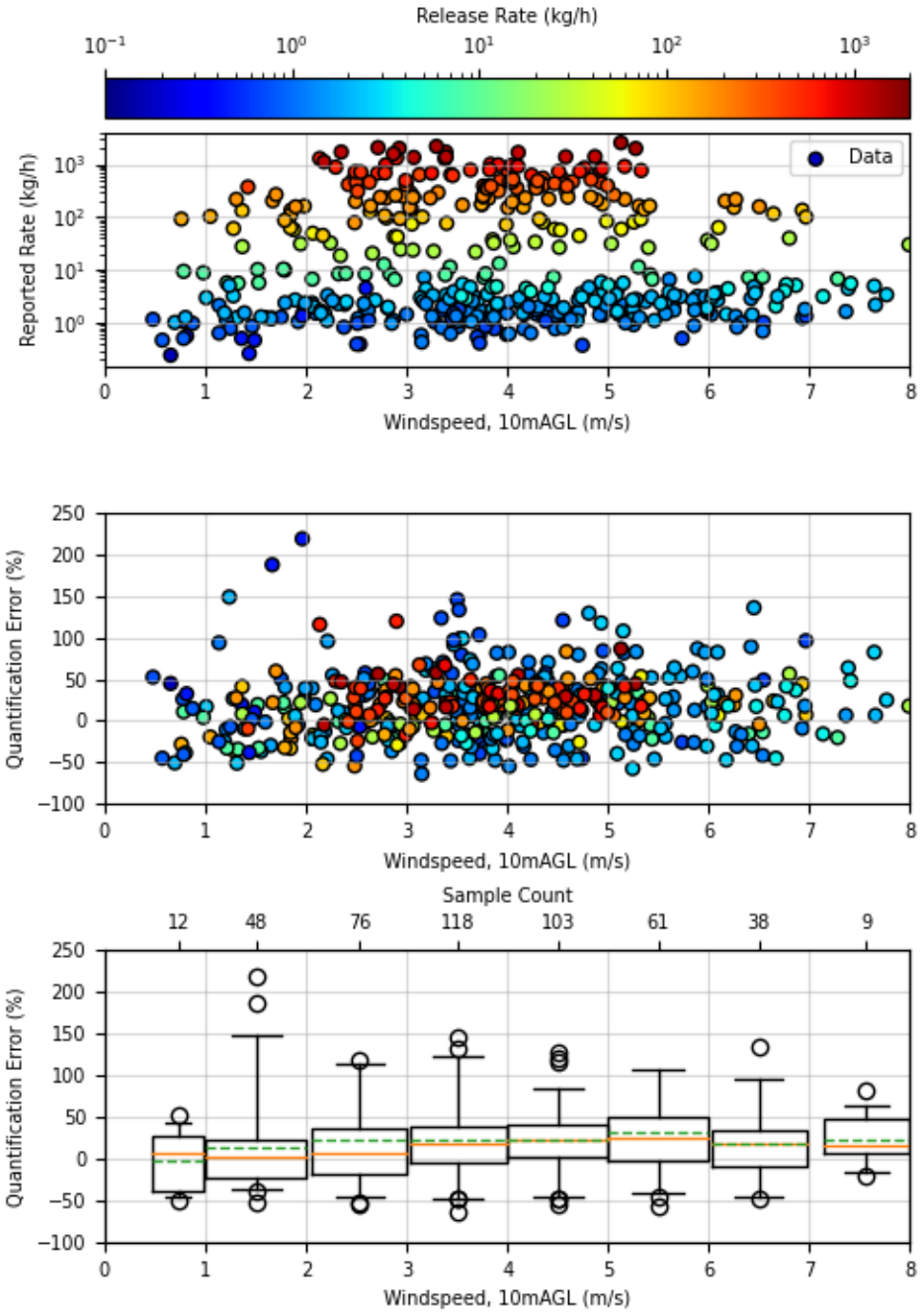

Figure 30. Accuracy of emission estimates produced with Sonic data vs windspeed. Marker colors represent the release rate. Error of individual measurements are shown as a percentage of the metered release rate (center panel). A box and whisker plot (lower panel) illustrates the mean (dashed line), median (solid line), inner quartiles (box), and 95% confidence (whisker) for data within each m/s wind category. Note, the y-limits of the center and bottom panels are set to a maximum of 250% error to improve visibility of the figures although 4 data points exceed 250% error. Only true positive detections are included in the figures and regression.

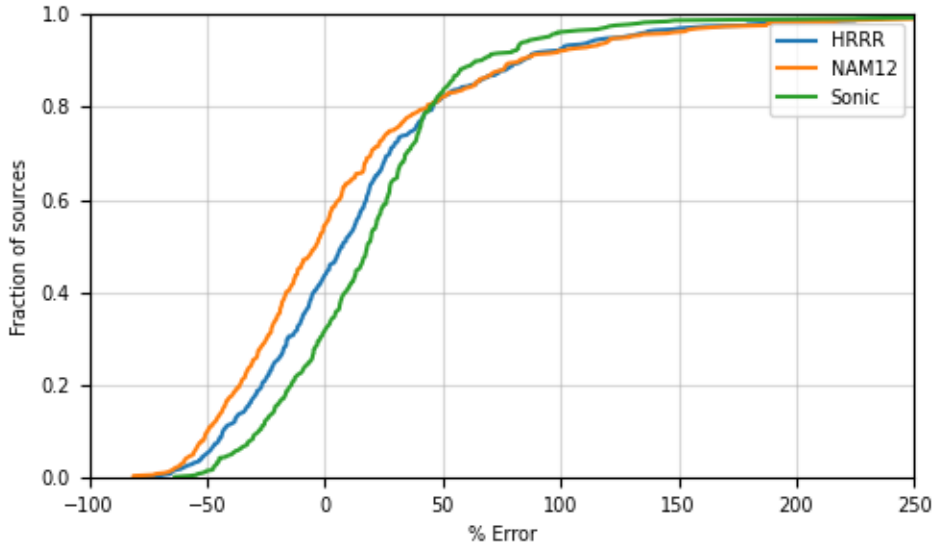

Figure 31. Distribution of error in emission rate estimates for each wind data source.

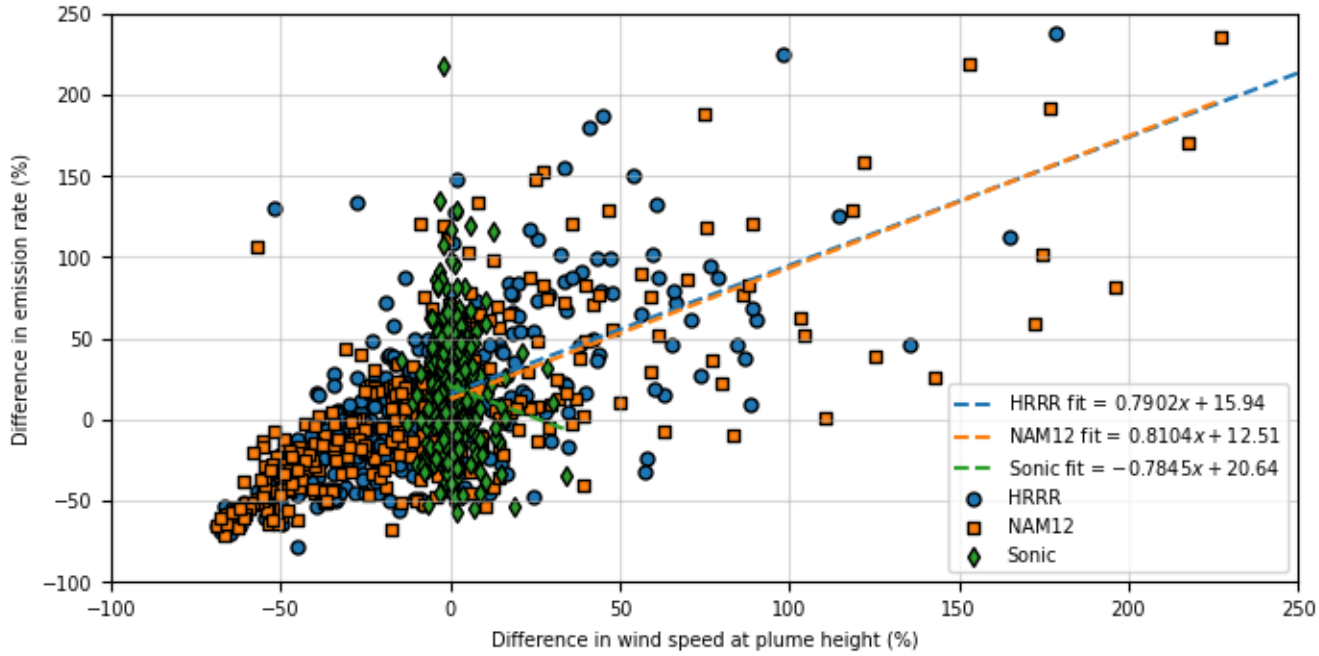

Figure 32. Error in emission rate estimate versus estimated error in wind speed at plume height for measurements performed at 675' AGL. For each wind source, the wind speed at the plume height was estimated using the sonic measurement data. The difference between the wind speed at plume height reported by bridger and the wind speed at plume height calculated by the study team is plotted on the x-axis. Generally, a positive correlation is seen across data where increasing error in the wind estimate results in increased error in the emission rate. However, data is present in all four quadrants (++, +-, –, and -+ error in wind and error in emission rate respectively).

Example Detections from Another Study

Table 3 reanalyzes data from the *Gathering Emission Factors Study*, file `AvgFactors.xlsx` Zimmerle et al. (2020) to illustrate the fraction of large emitters, by major equipment type and component type that could potentially be detected by the Bridger GML, provided they are emitted as a point source and form a clearly distinguishable plume. *Fraction of Emitters* indicates the fraction of detection emitters in each category, while *Fraction of Emissions* indicates the fraction of total emissions measured in each category. This analysis assumed 21 g/scf at 25 C / 1 atm, or approximately 16.8 g CH4/scf.

Table 3. Fraction of Emitters and Emissions Detectable for Gathering Compressor Stations

Equipment Category	Component Type	Fraction of Emitters >1 kg/h	Fraction of Emissions >1 kg/h	Fraction of Emitters >2 kg/h	Fraction of Emissions >2 kg/h
Tank	Common Multi-Unit Vent	36%	93%	19%	80%
Station	Common Station Vent	35%	91%	26%	80%
Compressor	Common Multi-Unit Vent	31%	87%	25%	80%
Compressor	Rod Packing Vent (NOP)	27%	75%	11%	41%
Compressor	Common Single-Unit Vent	23%	87%	17%	76%
Compressor	Rod Packing Vent (OP)	23%	78%	12%	62%
Compressor	Rod Packing Vent	23%	77%	11%	61%
Compressor	Valve	13%	73%	4.3%	56%
Tank	Common Single-Unit Vent	8%	65%	4.9%	56%
Tank	Thief Hatch	7.9%	61%	6.1%	54%
Compressor	Starter Vent	5.9%	97%	4.3%	96%
Compressor	Connector Threaded	5%	49%	2.2%	31%
Compressor	Regulator	2.7%	15%	0%	0%
Non-compressor	Valve	2.6%	31%	0.28%	4.8%
Compressor	Connector Flanged	2.4%	25%	1.6%	19%
Compressor	PRV	2.4%	62%	1.1%	43%
Non-compressor	PRV	2.2%	63%	0.61%	23%
Compressor	Pocket Vent	0.39%	3.3%	0%	0%
Compressor	Blowdown Vent	0.15%	11%	0.11%	10%
Compressor	OEL	0%	0%	0%	0%
Compressor	Rod Packing Vent (NOD)	0%	0%	0%	0%
Non-compressor	Connector Flanged	0%	0%	0%	0%
Non-compressor	Connector Threaded	0%	0%	0%	0%
Non-compressor	OEL	0%	0%	0%	0%
Non-compressor	Regulator	0%	0%	0%	0%

Data Availability

Data from this work is available on Dryad at https://doi.org/10.5061/dryad.ht76hdrkf. Data is organized such that each row corresponds to a single measurement pass by the aircraft. For each measurement pass controlled release data and meteorological data measured by the study team, and emission measurement data reported by Bridger Photonics are included. Three entries are included for each measurement pass; one for each wind dataset (HRRR, NAM12, and the local sonic

measurements) used by Bridger Photonics' in computing an emission rate estimate for the pass. A detailed description of each data column is included with the dataset.

References

Rutherford JS, Sherwin ED, Chen Y, Brandt AR. 2022. Controlled Release Experimental Methods: 2021 Stanford Controlled Releases in TX and AZ. https://eao.stanford.edu/sites/g/files/sbiybj22256/files/media/file/Method_description_Setup_and_Uncertainty_v18.pdf.

Zimmerle D, Vaughn T, Luck B, Lauderdale T, Keen K, et al. 2020. Methane Emissions from Gathering Compressor Stations in the U.S. *Environmental Science & Technology* **54**(12): 7552–7561. ISSN 0013-936X. doi:10.1021/acs.est.0c00516. https://doi.org/10.1021/acs.est.0c00516.